APD

An automated parameter determination system based on in-situ tests

Marzouk, Islam; Brinkgreve, Ronald; Lengkeek, Arny; Tschuchnigg, Franz

DOI
10.1016/j.compgeo.2024.106799

Publication date
2024

Document Version
Final published version

Published in
Computers and Geotechnics

Citation (APA)
Marzouk, I., Brinkgreve, R., Lengkeek, A., & Tschuchnigg, F. (2024). APD: An automated parameter determination system based on in-situ tests. *Computers and Geotechnics*, *176*, Article 106799. https://doi.org/10.1016/j.compgeo.2024.106799

Computers and Geotechnics 176 (2024) 106799

Contents lists available at ScienceDirect

Computers and Geotechnics

journal homepage: www.elsevier.com/locate/compgeo

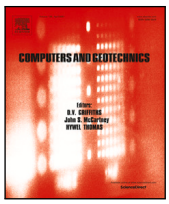

APD: An automated parameter determination system based on in-situ tests

Islam Marzouk [a,*], Ronald Brinkgreve [b], Arny Lengkeek [c], Franz Tschuchnigg [a]

[a] Institute of Soil Mechanics, Foundation Engineering and Computational Geotechnics, Graz University of Technology, Graz, Austria
[b] Delft University of Technology, Delft, The Netherlands
[c] Witteveen+Bos, Deventer, The Netherlands

ARTICLE INFO

Keywords:
CPT
DMT
V_s
FEM
In-situ testing
Graph theory
Soil parameters

ABSTRACT

In-situ testing has numerous applications in geotechnical engineering. The interpretation of in-situ test results includes soil stratification and determination of soil parameters. This paper presents an automated parameter determination framework that aims to determine constitutive model parameters based on in-situ tests. The ongoing research project relies on a graph-based approach for determining the parameters. The framework has two main attributes: transparency and adaptability. Transparency is achieved by illustrating how a certain parameter was computed. Adaptability is ensured by allowing users to incorporate their expertise into the framework. The system currently determines parameters based on three main workflows that utilize the results of cone penetration tests, dilatometer tests, and shear wave velocity measurements. This study employs the three main workflows to determine soil parameters for one of the Norwegian GeoTest Sites. Additionally, the connection between the parameter determination system and finite element analysis is discussed, where the parameters for the Modified Cam Clay model are evaluated. The framework is valuable in the early stages of projects, providing detailed soil information when soil data is limited. Ongoing research aims to assess the accuracy of the derived soil and constitutive model parameters and to expand the system's capabilities by including additional in-situ tests.

1. Introduction

The preference for numerical analysis over traditional methods stems from various reasons. One key benefit lies in the ability to achieve a higher level of detail, particularly in addressing geotechnical engineering problems like soil–structure interaction (Brinkgreve, 2019). Several factors impact the success of numerical analyses, with a key aspect being the proper determination of constitutive model parameters. Over the years, there has been significant development in soil constitutive models. Advanced models are able to accurately capture soil behaviour compared to simpler ones. However, as models become more sophisticated, the number of required parameters also increases. Generally, these parameters are inferred from laboratory tests (e.g., triaxial and oedometer tests) that are not always available in all projects.

In-situ tests can be considered as an alternative for determining soil parameters. When compared to laboratory testing, in-situ tests are faster, cheaper and (often) cause less soil disturbance. Nevertheless, it is not possible to determine soil parameters directly from the results of in-situ tests. Several empirical correlations exist to connect soil parameters to field measurements. However, due to the fact that various correlations have been proposed for the same soil parameter, a wide range of values can be obtained, increasing the uncertainty in the derived values. The reason for the uncertainty associated with correlations is embedded in the applicability of those correlations, as they are (often) only valid for specific soil types or conditions.

In literature, several guides are available for the interpretation of in-situ tests such as Kulhawy and Mayne (1990), Lunne et al. (1997b), Mayne (2014), Robertson (2015) for the cone penetration test (CPT), Marchetti et al. (2001) for the dilatometer test (DMT) and Mair and Wood (1987), Clarke (2022) for the pressuremeter test (PMT). There have been other approaches to determining constitutive model parameters based on very limited soil data such as Brinkgreve et al. (2010), where the parameters of the Hardening Soil Small Model (HSsmall) (Benz, 2007) were determined using only the relative density of the soil.

An ongoing research project aims to develop an automated parameter determination (APD) framework designed to identify constitutive model parameters based on in-situ tests. This is extremely useful in the early stages of projects when limited soil data is available. At this stage, (relatively inexpensive) field tests such as CPT and DMT are carried out prior to a full laboratory test campaign. However, by using APD in the pre-design phase of the project, users can efficiently obtain much

* Corresponding author.
E-mail address: islam.marzouk@tugraz.at (I. Marzouk).

https://doi.org/10.1016/j.compgeo.2024.106799

Available online 7 October 2024

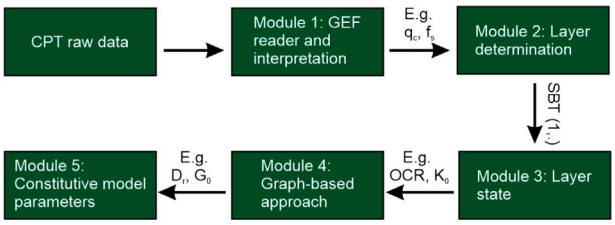

Fig. 1. Overview of modules, used for automated parameter determination.

more detail. The motivation is not to replace laboratory tests with in-situ tests. They will still be needed to improve the soil and constitutive model parameters for the final design.

In APD, the parameters are computed using a graph-based approach. This approach inherits some of the properties of graph theory (Van Berkom et al., 2022). The main objective of the project is to formulate a parameter determination system that is transparent and adaptable. The former is achieved by illustrating how the values obtained for different parameters were calculated based on the available information, while the latter is ensured by allowing the users of the system to incorporate their experience and expertise into the system.

In Section 2, the framework and the different modules of APD are illustrated. The in-situ tests considered are shown in Section 3. A case study where the soil parameters were assessed based on CPT, DMT and shear wave velocity measurements is presented in Section 5. The transition from soil parameters to constitutive model parameters is highlighted in Section 6. Finally, the conclusions and next steps are discussed in Section 7.

2. Automated Parameter Determination framework

The parameter determination framework is built in the programming language Python. The system consists of sequential modules that link raw data (field measurements) to constitutive model parameters. In the case of computing parameters from CPT, the five modules are shown in Fig. 1. The 1st module imports the field measurements. The measurements are then transferred to the 2nd module where the CPT is stratified. The stratified layers are sent to the 3rd module where the state of the layers is determined (overconsolidation ratio (OCR) and coefficient of earth pressure at rest (K_0)). Soil parameters are determined for each layer in the 4th module, while the constitutive model parameters are evaluated in the 5th module. The five modules are described in detail in Sections 2.1–2.4, respectively.

2.1. Module 1

The Geotechnical Exchange Format (GEF) is one of the standard formats for CPT files. After importing the raw data, the measurements, cone tip resistance (q_c), sleeve friction (f_s) and pore water pressure measurements (u_2) - in the case of piezocone (CPTu) - are stored as data frame (data structure in Python). In addition, Module 1 automatically interprets the cone tip net area ratio (a) and the groundwater level from the GEF file. If this information is missing, it can be added manually by the user.

The raw measurements are used to compute CPT parameters in the next step. These parameters comprise the corrected cone tip resistance (q_t) and the friction ratio (R_f). For other CPT parameters, the total unit weight (γ_t) needs to be evaluated to calculate the vertical stress (total and effective). This unit weight is defined as the initial unit weight. It can be calculated according to Robertson and Cabal (2010) as follows:

$$\gamma_t = \gamma_w[0.27(\log R_f) + 0.36(\log q_t/p_a) + 1.236] \quad (1)$$

It should be noted that other correlations/values could also be used for the total unit weight. For instance, if the correlation proposed by Lengkeek and Brinkgreve (2022) (Eq. (2)) is used, the unit weights (particularly for organic soils) would differ, resulting in varying stresses and therefore different CPT normalized parameters. Users could also use values based on experience or based on laboratory test results. Moreover, in module 4 (see Section 2.4), additional correlations are used for the total unit weight and the user can compare the values obtained from different correlations and further update the initial unit weight used in this module. The variations in unit weight resulting from the use of different correlations (or from using experience values) and the variations in the resulting soil stress profile have a relatively minor influence on the inherent variability of outcomes from correlations that are subsequently employed in the parameter determination process.

$$\gamma_t = 19.5 - 2.87[\frac{\log(\frac{9000}{q_t})}{\log(\frac{20}{R_f})}] \quad (2)$$

Additional CPT parameters are then evaluated such as the normalized friction ratio (F_r), pore pressure parameter ratio (B_q), normalized cone resistance (Q_t), normalized cone resistance corrected for stress level (Q_{tn}) and the normalized soil behaviour type (SBT) index (I_{cn}). The definition of these CPT parameters is illustrated in several CPT guides, such as Robertson (2015).

2.2. Module 2

The stratification is based on the soil behaviour type (SBT) charts. The SBT is determined using one of the following three charts:

- Robertson's normalized SBT chart (Robertson, 2009)
- Robertson's modified non-normalized SBT chart (Robertson, 2010)
- Robertson's updated normalized SBT chart (Robertson, 2016)

The SBT is determined for each CPT measurement (e.g. Table 1 shows the SBT for Robertson's 2010 non-normalized SBT chart). There are currently three approaches to creating layers from CPT measurements. The first two approaches rely on algorithms that group subsequent CPT measurements with preferably the same SBT together. Layer boundaries are created whenever a major transition can be noticed from one SBT to another. In this way, the entire CPT is divided into a limited number of layers, each represented by their overall averaged SBT. The last approach is a manual stratification, where the user specifies the boundaries of the layers and these boundaries are taken into account in the stratification. Other (automated) stratification approaches from literature (e.g. Brinkgreve et al. (2023)) can also be applied. In general, any method could be used in an automated system. In this paper, the results (Section 5) are presented based on manual stratification to generate an adequate number of layers covering the in-situ test soundings for comparison with reference values of different parameters. Therefore, the stratification approaches are not discussed in detail in this contribution.

After the determination of the layers, the raw data as well as the CPT parameters (presented in 2.1) are averaged within each layer. These averaged values act as the representative values for the layers. The parameters in modules 4 and 5 (Section 2.4) are assessed based on these averaged values.

2.3. Module 3

The layer state in the current version of APD is determined by computing initial values for OCR and K_0. The initial value of OCR can be computed according to Mayne et al. (2009) as follows:

$$OCR = \frac{\sigma'_p}{\sigma'_v} = \frac{0.33(q_t - \sigma_v)^{m'}}{\sigma'_v} \quad (3)$$

Table 1
SBT zones according to Robertson (2010).

Zone	Soil Behaviour Type (SBT)
1	Sensitive fine-grained
2	Clays – organic soil
3	Clays: clay to silty clay
4	Silt mixtures: clayey silt & silty clay
5	Sand mixtures: silty sand to sandy silt
6	Sands: clean sands to silty sands
7	Dense sand to gravelly sand
8	Stiff sand to clayey sand (overconsolidated)
9	Stiff fine-grained (overconsolidated)

where σ'_p is the preconsolidation stress and m' is the yield stress exponent that increases with fine content and decreases with mean grain size. Mayne (2017) suggested determining m' from I_{cn} as follows:

$$m' = 1 - \frac{0.28}{1 + (\frac{I_{cn}}{2.65})^{25}} \tag{4}$$

The initial value of K_0 may be evaluated according to Kulhawy and Mayne (1990) as follows:

$$K_0 = 0.5 \times OCR^{0.5} \tag{5}$$

Similar to the initial value for the total unit weight (Eq. (1)), the correlations presented in Eqs. (3) and (5) can be changed according to the user's preference. Moreover, additional correlations for OCR and K_0 are used in module 4 (Section 2.4). Thus, the user can update the values used in module 3 based on the results obtained in module 4.

2.4. Modules 4 and 5

Modules 4 and 5 are utilized to compute both soil and constitutive model parameters using a graph-based approach. As both modules are formulated in the same way and operate at the same time, they are both discussed in the same section.

2.4.1. Graphs as a parameter determination tool

Graph theory is a branch of discrete mathematics that studies the relationships between objects in a network. In this context, a graph serves as the mathematical representation of a network and is defined by two sets of elements: nodes, which represent the entities within the graph, and edges, which represent the connections between pairs of nodes. Graphs are useful for visually representing complex systems, such as transportation networks (Likaj et al., 2013) and social media (Chakraborty et al., 2018). The APD framework is based on a weighted directed graph, where each pair of nodes in the graph has an inherent direction, and edges connecting nodes can have a weight. An example of a weighted directed graph is a one-way road, where weights can be assigned to the roads (edges), indicating distance or travel time (Van Berkom et al., 2022).

Fig. 2 illustrates the basic concept of the graph-based approach implemented in APD: source parameters (CPT raw data) are connected to destination parameters (soil or constitutive model parameters) through intermediate parameters. This is achieved based on a given set of correlations. The system generates all the paths (chains of correlations) connecting source parameters to destination parameters. Moreover, it determines the value(s) of the intermediate/destination parameters. Within the framework of APD, the general term 'method' substitutes the terms of 'correlation', 'formula', 'equation' and 'rule of thumb'. The graphs are generated using the Python graph visualization library *graphviz* (Gansner, 2011).

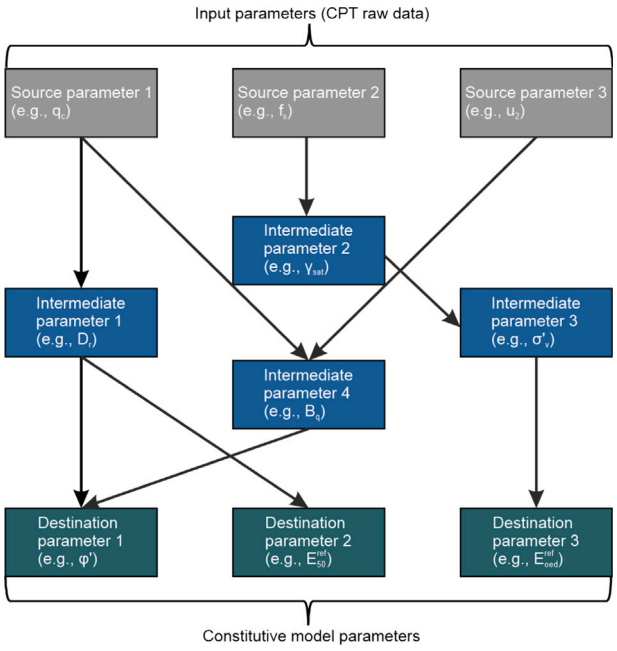

Fig. 2. Graph-based approach implemented in APD.

2.4.2. Differences to classical graph theory

Searching for a path in a network from one node to another is a common problem that has been used in different applications (Shu-Xi, 2012). Several graph algorithms exist for solving the shortest path problem (e.g., Dijkstra's algorithm (Dijkstra, 1959)). However, those algorithms are not valid for the parameter determination framework as they cannot be applied to branching paths. In APD, a path to the destination node can have more than one source node as the parameters in the path can be obtained from multivariable formulas that depend on multiple input parameters (branching paths occur in the framework). However, in graph theory, a path is defined as the connection between a pair of nodes (there are no branching paths). In addition, as there are several methods to determine the same parameter in APD, it is often the case that more than one branching path can lead to the destination parameter. As a result, the existing graph algorithms are not suitable for the parameter determination framework (Van Berkom et al., 2022).

To overcome the issue with branching paths, two types of nodes are introduced. One node defines the parameters, while the other node represents the methods. The motivation for this solution is illustrated by the following example. Consider the following two methods (correlations) according to Lunne and Christoffersen (1983) and Kulhawy and Mayne (1990), respectively, to compute the relative density (D_r) from the CPT.

$$D_r = (1/2.91)\ln(q_c/61(\sigma'_v)^{0.71}) \tag{6}$$

$$D_r = 100\sqrt{Q_{tn}/(305 \times OCR^{0.2})} \tag{7}$$

Eqs. (6) and (7) are named as 'method_Dr_1' and 'method_Dr_2', respectively. It is clear that each method is a multivariable formula, where Eq. (6) requires q_c and σ'_v as inputs and Eq. (7) requires Q_{tn} and OCR as inputs. Fig. 3a presents the above-mentioned example while using only one type of node, parameters. Clearly, this visualization does not show that there are two unique paths to compute D_r. On the other hand, Fig. 3b shows the same example when two types of nodes are used, parameters and methods. This representation clearly shows that there are two unique paths to determine D_r. Moreover, it explicitly visualizes that for 'method_Dr_1', q_c and σ'_v are the inputs, while for 'method_Dr_2' Q_{tn} and OCR are the inputs.

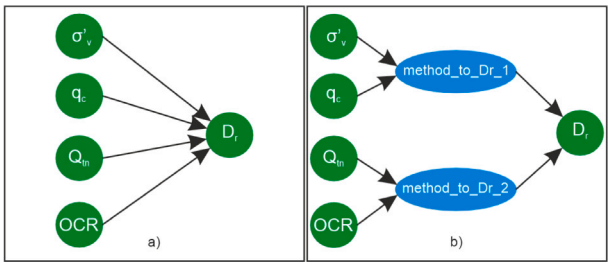

Fig. 3. Representation of multivariable formulas (a) one type of node (b) two types of nodes.

The methods are considered as an external input to the system (as discussed in 2.4.3). The system contains only the algorithm for creating paths between methods and parameters that share a connection. By formulating the system in this way, it is modular and adaptable, as the external input to the system depends on the user's knowledge, experience and preferences.

2.4.3. Generating the graph

The graphs are generated based on the parameters, methods and the connection between them. This is achieved by providing the system with input files in comma-separated value format (CSV). The two files contain the methods and the parameters. Each file consists of special properties that need to be defined to create the links between the methods and parameters and to generate the graph.

To illustrate these properties, Eq. (6) is used as an illustrative example for creating CSV files for the methods and parameters. The corresponding files for this method as well as the generated graph are presented in Fig. 4.

Starting by the methods CSV file, the following properties need to be defined: *method_to*, *Formula*, *parameters_in*, *parameters_out*, *validity* and *Reference*. The *method_to* field contains the name of the method, in this case method_to_Dr. The following field contains the formula of the method (Eq. (6)), note that "ln" is not recognized in the environment of Python; hence "log" (which is log with base e) is used in Fig. 4. The input parameters of the method (q_c and σ'_v) are defined in *parameters_in*, while the output of the method (D_r) is stated in *parameters_out*. The *validity* field defines the applicability of the method. As some methods are applicable to all soil types, others are only valid for either coarse or fine grained soils. The *validity* is based on the modified non-normalized Robertson's chart (Robertson, 2010). The *validity* for methods is defined according to Table 1. For example, if the method is only valid for silts, the *validity* should be set to SBT(4). Regarding the example in Fig. 4, as the relative density concerns coarse-grained soils, the *validity* is set to SBT(5678) (refer to Table 1). In addition to SBT, other parameters such as B_q can be used as validity criterion. In case the method is limited to B_q values in the range [0.1, 1.0], this can be indicated as Bq_min(0.1) Bq_max(1.0). If B_q values fall outside this range, the method will not be considered. The author of the method can optionally be mentioned in the *Reference* field.

For the parameters CSV file, the following properties need to be defined: *Symbol*, *Description*, *Unit*, *Value* and *Constraints*. The parameters CSV file simply contains all of the parameters that have been used in the methods CSV file (in the fields of *parameters_in* and *parameters_out*). The *Symbol* field follows the same notation used in the fields of *parameters_in* and *parameters_out* fields of the methods CSV file. The other fields in the parameters CSV file are optional, where the user can specify the name of the parameter in the *Description* field. It is recommended to add the unit of all parameters in the *Unit* field to avoid mistakes due to unit conversions. The *value* field sets a specific value for the parameter. This value is specified manually by the user (e.g., unit weight of water), otherwise it should be empty as the value is calculated by the system. The *constraints* field applies upper and lower bounds to the parameter. If the system calculates a value higher than the upper bound or lower than the lower bound, this value is discarded. For example, in Fig. 4, a lower bound of 0% and an upper bound of 100% is set for the relative density.

By creating the two CSV files following the above-mentioned format, the system imports the files and creates the connections between methods and parameters. Consequently, a graph presenting the linkage between parameters and methods is generated. Furthermore, the value(s) for different parameters are computed.

2.4.4. Correlations database

The correlations database is an external input to the system. The user of the system is responsible for providing the methods that would be used to compute the parameters. Nevertheless, a standard validated database of methods and parameters is provided alongside APD. This database is continuously updated and improved. Even when using the provided standardized database, the users should still apply their experience and knowledge to the output of the system. Nonetheless, the system should produce 'reasonable' value(s) for different parameters.

As discussed in Section 3, currently APD consists of three main workflows. The parameters could be assessed based on CPT (Section 3.1), DMT (Section 3.2) and shear wave velocity measurements (Section 3.3). Consequently, three validated databases of methods and parameters are provided for the three workflows. These databases contain over 200 methods. It should be noted that both methods for soil and constitutive model parameters are present in the same database.

3. In-situ tests considered

3.1. CPT-based workflow

CPT is increasingly being used in comparison to other in-situ tests. Additionally, the CPT results are continuous (measurements are taken every 1 to 2 cm), which is advantageous for the stratification of the CPT profile into soil layers. In addition, several measurements are obtained (q_c, f_s and u_2 in the case of CPTu). In the literature there are several correlations that relate the CPT measurements to different soil parameters. On the other hand, this increases the uncertainty in the derived values, as the large number of correlations leads to a wide range of values for the parameter of interest. The architecture of the CPT-based workflow is shown in Fig. 1.

3.2. DMT-based workflow

The DMT-based workflow is formulated similarly to the CPT-based workflow (Fig. 1). Firstly, DMT raw data is imported by the DMT reader (1st module, see Section 3.2.1). Afterwards, DMT measurements are transferred to the 2nd module (DMT layer interpretation), where layers are identified. Marchetti's chart (Fig. 5) (Marchetti and Crapps, 1981) for estimating the soil type is used to determine the SBT for each DMT measurement. Marchetti's chart is divided into 4 different zones, mud/peat, clay, silt, and sand as shown in Table 2.

3.2.1. DMT module 1

Similar to CPT module 1 (Section 2.1), the intermediate DMT parameters are computed within DMT module 1. These parameters are required to use Marchetti's soil type and unit weight chart (Fig. 5) and to compute other parameters.

The raw measurements in the form of the corrected first and second readings (P_0 and P_1, respectively) are imported by the DMT reader. They are used to derive the intermediate DMT parameters: the material index ($I_D = \frac{P_1-P_0}{P_0-u_0}$) and the dilatometer modulus $E_D = 34.7(P_1 - P_0)$. The other intermediate DMT parameter, the horizontal stress index ($K_D = \frac{P_0-u_0}{\sigma'_v}$) requires the determination of the effective vertical stress, which in turn requires the determination of the unit weight. Consequently, an initial estimate of the unit weight is required (similar

Methods CSV file

method_to	Formula	parameters_in	parameter_out	validity	Reference
method_to_Dr	(1/2.91)log(q_c/61(σ'_v)$^{0.71}$)	q_c, σ'_v	D_r	SBT(5678)	LunneChristoffersen_1983

Parameters CSV file

Symbol	Description	Unit	Value	Constraints
D_r	Relative density	%		lower_bound(0) upper_bound(100)
q_c	Cone tip resistance	kPa		
σ'_v	Vertical effective stress	kPa		lower_bound(0)

Generated graph

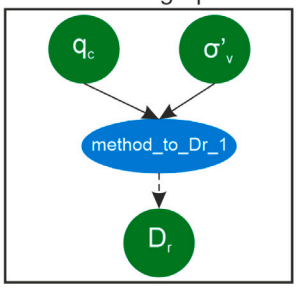

Fig. 4. Format of methods and parameters CSV files.

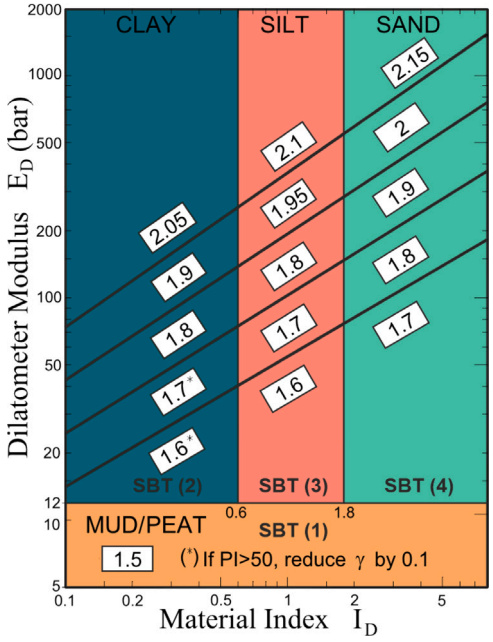

Fig. 5. Marchetti's chart for soil type and unit weight (Marchetti and Crapps, 1981).

Table 2
SBT according to Marchetti's soil type chart.

SBT	Soil type
Mud/peat	1
Clay	2
Silt	3
Sand	4

to CPT module 1). The initial unit weight can be determined using Marchetti's chart (Marchetti and Crapps, 1981) (Fig. 5). This value can be updated based on available data or based on the results of module 4.

3.2.2. Other DMT modules

The other DMT modules follow the same format as the CPT modules illustrated in Sections 2.2–2.4. DMT module 2 focuses on stratification, which is based on Marchetti's chart (Fig. 5). Each of the four main zones in Marchetti's chart is assigned a different SBT, as depicted in Fig. 5. Similar SBTs are grouped together to form larger layers. The DMT stratification algorithm is currently being investigated and compared with the CPT stratification approaches. Additionally, similar to module 2 of the CPT-based workflow, manual DMT stratification is possible. As mentioned above, the analysis in this contribution is based on manual stratification.

DMT module 3 computes initial values for OCR and K_0. The user can select any method for computing these values. Section 4.3 presents some DMT methods for computing OCR. Modules 4 and 5 are identical to the CPT-based workflow (as discussed in Section 2.4).

3.3. Shear wave velocity-based workflow

In recent years there has been an increase in the use of seismic tests such as Seismic Dilatometer Test (SDMT) and Seismic Cone Penetration Test (SCPT/SCPTu). The main motivation for creating this workflow is to directly use the in-situ measured shear wave velocity (V_s) to accurately determine the small-strain shear modulus (G_0), thus removing the uncertainty in using shear wave velocity correlations to determine V_s and G_0.

As it is often the case that the in-situ shear wave velocity measurements are part of an SDMT or SCPT sounding, the shear wave velocity workflow can be seen as complementary (add-on) to either the CPT or DMT workflows. However, it is possible to use other measurements of V_s in the shear wave velocity-based workflow. The in-situ shear wave velocity measurements are imported by the system and the layers are provided by the user. The shear wave velocity measurements are averaged within each layer and the average value is used as the representative shear wave velocity for that layer. As a result, the shear wave velocity is considered as a source parameter in this workflow rather than an intermediate parameter (as in the CPT-based workflow).

3.3.1. Shear wave velocity modules

The V_s-based workflow is complementary to either the CPT or DMT workflows and follows the same module definition. If used with the CPT-based workflow, CPT modules 1, 2, 3, 4 and 5 are employed. The same applies to the DMT-based workflow.

3.3.2. Layers without shear wave velocity measurements

Implementing the shear wave velocity add-on within the APD framework presents a challenge due to stratification. APD evaluates parameters based on layers, while shear wave velocity recordings have larger intervals (often 0.5 to 1 m) compared to CPT (1 or 2 cm) and DMT (20 cm). As a result, some layers may not include V_s measurements, thus the shear wave velocity workflow would be unusable for the entire analysis.

In order to overcome this limitation, a number of approaches are currently being investigated. One such approach involves the utilization of machine learning algorithms for the purpose of predicting missing

shear wave velocity data, as presented in Felić et al. (2024). An alternative approach is to utilize site-specific CPT V_s methods (correlations), whereby multiple V_s methods are compared to the in-situ V_s profile, and the method with the least error is employed to predict the missing data points. This approach has been implemented and is currently under investigation, with its efficacy being verified through its application to a range of cases. In the present study, these approaches were not employed, as in-situ V_s measurements were available for all layers under consideration.

At the present time, the V_s-based workflow is employed solely for the purpose of reliably inferring small-strain parameters for the layers where V_s measurements are available. The resulting parameters, which are reliable, can be used as additional source parameters in the other workflows, thereby reducing the uncertainty in some of the computed parameters.

4. Application of APD on the Onsøy site

This section describes the use of the APD system for the calculation of soil parameters for a test site, using the described three main workflows: CPT, DMT and V_s. The test site is described in Section 4.1, while the parameters are illustrated in Sections 4.2–4.5. Only some selected methods were used to assess these parameters, as described in the corresponding subsections.

4.1. Test site

Data for this analysis was gathered from one of the Norwegian GeoTest Sites (NGTS) using the web-based application 'Datamap'.

4.1.1. Datamap

The web application 'Datamap' has been developed to capture, classify, and organize geotechnical data. It provides a platform for making geotechnical data available and allows researchers to create and share their projects. The application can be accessed through www.geocalcs.com/datamap (Doherty et al., 2018).

4.1.2. Norwegian GeoTest Sites (NGTS)

Between 2016 and 2019, the Norwegian Geotechnical Institute (NGI), the Norwegian University of Science and Technology (NTNU), SINTEF Building and Infrastructure, the University Centre in Svalbard (UNIS), and the Norwegian Public Roads Administration (NPRA) established five GeoTest Sites (NGTS) in Norway. These sites correspond to different soil types, including clay, silt, quick clay, sand, and permafrost (L'Heureux and Lunne, 2020).

4.1.3. Onsøy soft clay

The NGTS soft clay site at Onsøy was established in 2016. An extensive laboratory and field testing program has been conducted and is presented in NGI's report (Norwegian Geotechnical Institute 2019). In-situ testing included piezocone tests (CPTu), seismic cone penetration tests (SCPT), a seismic flat dilatometer test (SDMT), and a self-boring pressuremeter test (SBPMT). The laboratory testing comprised of determining the in-situ water content, unit weight, Atterberg limits and executing constant rate of strain oedometer tests (CRS), triaxial tests and direct simple shear tests (DSS). Block and various types of tube samplers were used for sample recovery (Gundersen et al., 2019).

The investigation focused on two main areas: south-central (SC) and southeast corner (SEC). The layout of the test site is illustrated in Fig. 6, highlighting the two areas. The test site's stratigraphy comprises four slightly overconsolidated main units (Gundersen et al., 2019). Unit I is composed of weathered clay, while Unit II is characterized as a clay with a high to very high plasticity index (approximately 44%). Unit III is identified as a clay with a medium-high plasticity index (approximately 27%). Unit IV exhibits similar index properties to Unit II, although the plasticity index, water content, and clay content decrease towards the bedrock. This analysis only considers the southeast corner (SEC) area, where the SDMT was conducted (see Fig. 6). Unit I is 1 m thick, Unit II is approximately 9.5 m thick, and Unit III is 9 m thick (Gundersen et al., 2019).

Fig. 7 presents the in-situ tests selected as input for APD. The results of the selected CPTu (ONSC18 in the project (see Fig. 6)) in terms of the cone tip resistance (q_c), sleeve friction (f_s) and pore pressure measurements (u_2) are shown in Figs. 7(a–c), while the results of the selected seismic dilatometer test (SDMT) (ONSD01 in the project (see Fig. 6)) in terms of the corrected pressure readings (P_0 and P_1) and shear wave velocity (V_s) are shown in Figs. 7(d–e). The four different soil units are also highlighted in the figures.

The selected CPTu had a 10 cm^2 compression cone and a 150 cm^2 friction sleeve. The pore pressure transducer was located in the u_2 position and the CPTu measurements were recorded every 1 cm. The SDMT measurements were taken every 20 cm, while the shear wave velocity was measured every 50 cm.

The CPT-based workflow has been used to determine soil parameters for this site in Marzouk et al. (2023a). While the DMT-based workflow was employed to evaluate soil parameters for the same site in Marzouk et al. (2023b).

4.2. Unit weight

The need for an initial estimate of the unit weight is discussed in module 1 (see Section 2.1). Some selected methods for the unit weight for the 3 workflows are presented in Table 3.

The initial unit weight can be defined using any method or value. In this analysis, Eq. (2) was used to calculate the initial unit weight for both the CPT and V_s-based workflows. Similarly, unit weight obtained from Fig. 5 was selected as the initial unit weight for the DMT-based workflow. The impact of the unit weight on the calculated parameters is briefly discussed in Section 5.1.

4.3. Stress history

The stress history is commonly defined based on the overconsolidation ratio (OCR). The methods chosen for computing OCR are presented in Table 4. It should be noted that the effective vertical stresses required for some of these methods are calculated based on the initial unit weight (discussed in Sections 2.1 and 4.2).

4.4. Stiffness parameters

The 1-D constrained tangent modulus (E_{oed}) is often used to predict settlements. The methods selected for assessing E_{oed} are illustrated in Table 5. The value of α_M in Eq. (31) is presented for the case of $I_{cn} > 2.2$ and $Q_{tn} < 14$, as all the layers evaluated for the CPT analysis had I_{cn} values greater than 2.2 and Q_{tn} less than 14. Similarly, the correction factor R_M in Eq. (32) is presented for the case of $I_D \leq 0.6$, as all the layers evaluated for the DMT analysis had I_D values less than 0.6.

The small-strain shear modulus (G_0) is determined from V_s using Eq. (46), where ρ represents the soil density. Table 7 presents the methods chosen for determining G_0. It is important to note that for the CPT-based workflow, G_0 is determined using Eq. (46), where the values of V_s are calculated from methods presented in Table 6.

4.5. Strength parameters

Table 8 presents the selected methods for determining the undrained shear strength (s_u). Bearing factors for net tip resistance, excess pore-water pressures and effective cone resistance are denoted by N_{kt} (Eqs. (47–48)), $N_{\Delta u}$ (Eqs. (49–50)), and N_{ke} (Eqs. (51–52)), respectively. Average values of 12, 6, and 8 could be selected for N_{kt} (Eq. (47)), $N_{\Delta u}$ (Eq. (49)) and N_{ke} (Eq. (51)), respectively (Mayne, 2016). Several researchers concluded that N_{kt} and N_{ke} vary inversely with B_q (Eq. (48) and Eq. (52)), while $N_{\Delta u}$ varies directly with B_q earchers co (Eq. (50)) (Mayne et al., 2023).

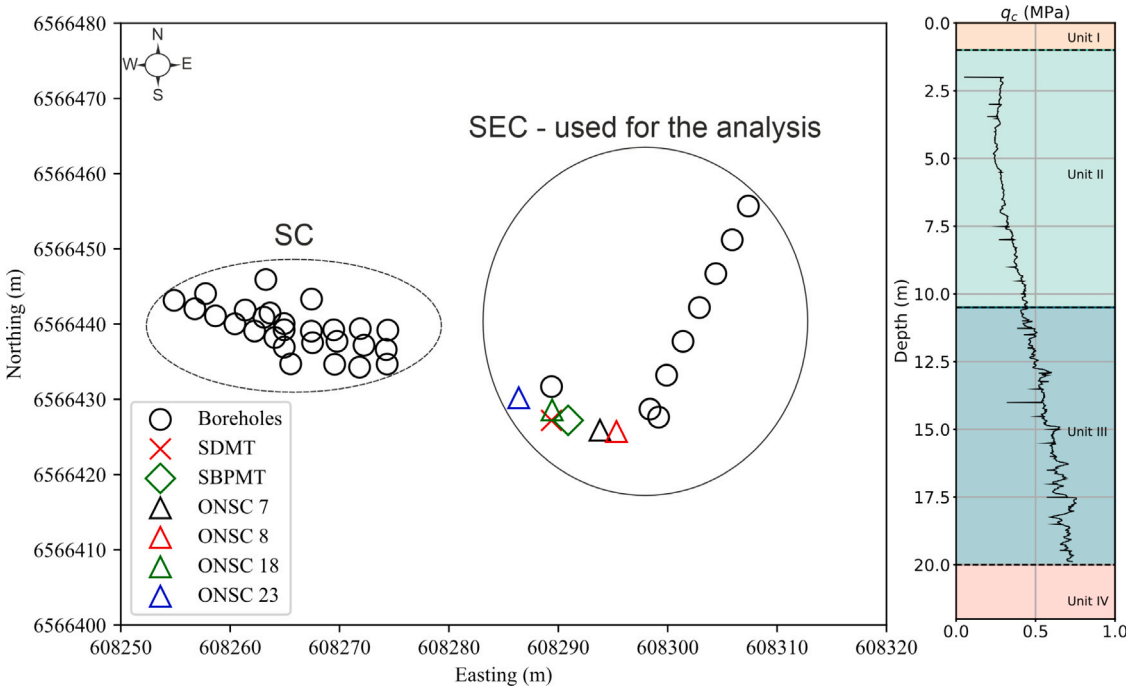

Fig. 6. Layout of the test site and stratification of SEC area.

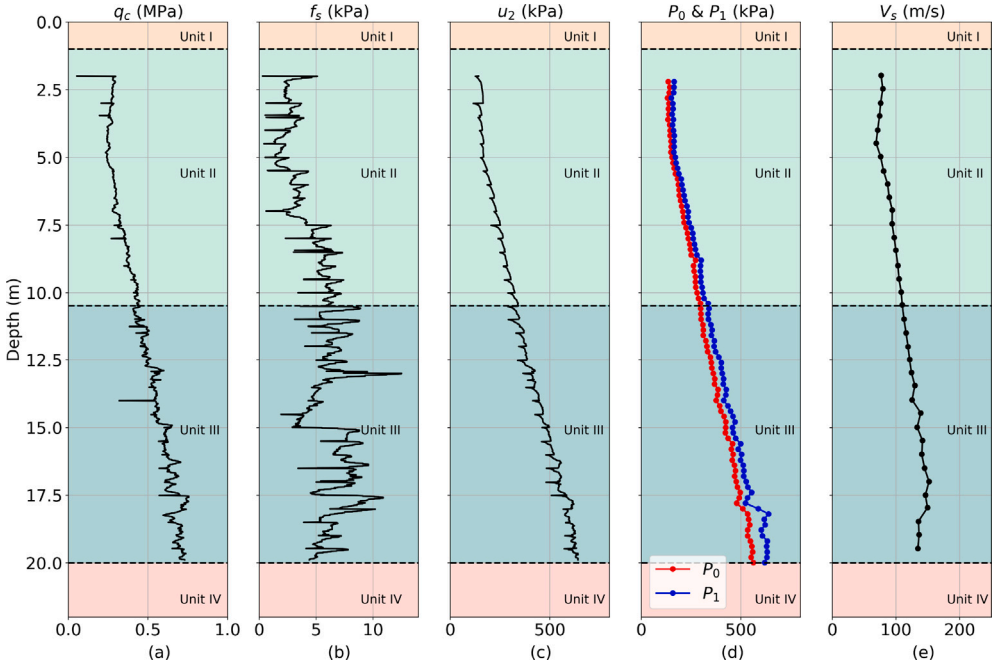

Fig. 7. Results of selected in-situ tests, (a–c): CPTu results (profiles of q_c, f_s and u_2); (d): DMT results (P_0 and P_1); (e): V_s profile from the SDMT.

5. Results and validation

Sections 4.2 to 4.5 presented the selected methods for determining soil parameters for the CPTu and SDMT illustrated in Fig. 7. It should be noted that there are many more methods available in the APD database. The methods presented in the previous subsections have been selected to illustrate the workflow and show the potential of APD. In this study, CPTu and SDMT results were averaged every 1 m (manual layering) and these values were used as input for the analysis. The purpose of this process (manual layering and averaging) is to generate an adequate number of layers that cover the in-situ test soundings for comparison with the reference values of different parameters. The APD generally computes parameters based on layers, therefore selecting layers with smaller thickness would result in a larger number of layers and subsequently, a larger number of graphs. This would, of course, make the interpretation of parameters a more time-consuming process. As a result, layers with a thickness of 1 meter were chosen.

Since the layers are determined manually, the user must provide the SBT for each layer. This SBT will act as a validity criterion for the methods CSV file. In this study, the test site is a homogeneous soft clay deposit. Consequently, all the layers had SBT(3) corresponding to clay, according to Robertson (2010) (refer to Table 1). The averaging

Table 3
Selected methods for the unit weight (γ_t).

Workflow	Method		Author
CPT	$\gamma_w[0.27(\log R_f) + 0.36(\log q_t/p_a) + 1.236]$	(1)	Robertson and Cabal (2010)
	$19.5 - 2.87[\frac{\log(\frac{9000}{q_t})}{\log(\frac{20}{R_f})}]$	(2)	Lengkeek and Brinkgreve (2022)
	$26 - \frac{14}{1 + [0.5\log f_s + 1]^2}$	(8)	Mayne (2014)
	$0.254 \cdot \log(\frac{q_t - u_2}{p_a}) + 1.54$	(9)	Mayne et al. (2023)
DMT	from Marchetti's chart	(Fig. 5)	Marchetti and Crapps (1981)
	$\gamma_w \cdot 1.31(\frac{P_1}{p_a})^{0.161}$	(10)	Ozer et al. (2012)
	$\gamma_w \cdot 1.35(\frac{P_0}{p_a})^{0.159}$	(11)	Ozer et al. (2012)
	$\gamma_w \cdot 1.32(\frac{P_1}{p_a})^{0.091}(\frac{P_0}{p_a})^{0.0733}$	(12)	Ozer et al. (2012)
	$\gamma_w \cdot 1.47(\frac{E_D}{p_a})^{0.045}$	(13)	Ozer et al. (2012)
V_s	$8.31\log V_s - 1.61\log z$	(14)	Mayne (2001)
	$4.17\ln V_{s1} - 4.03$	(15)[a]	Mayne (2007)
	$\frac{6.87V_s^{0.227}}{\sigma_v'^{0.057}}$	(16)	Burns and Mayne (1996)
	$4.96 + 5.97\log V_s$	(17)	Duan et al. (2019)

[a] V_{s1} is the effective stress-normalized shear wave velocity ($V_{s1} = V_s/(\sigma_v'/p_a)^{0.25}$).

Table 4
Selected methods for the overconsolidation ratio (OCR).

Workflow	Method		Author
CPT	$\frac{0.33(q_t - \sigma_v)^{m'}}{\sigma_v'};\ m' = 1 - \frac{0.28}{1 + (\frac{I_{cn}}{2.65})^{25}}$	(18)	Mayne et al. (2009), Mayne (2017)
	$0.25Q_t^{1.25}$	(19)	Robertson (2009)
	$0.2 + 0.39Q_t$	(20)	Paniagua et al. (2019)
	$1.02B_q^{-1.077}$	(21)	D'Ignazio et al. (2019)
	$0.63B_q^{-1.286}$	(22)	Schroeder et al. (2006)
DMT	$(0.5K_D)^{1.56}$	(23)	Marchetti (1980)
	$2(\frac{P_0 - \sigma_v}{6.63\sigma_v'})^{1.19}$	(24)	Cao et al. (2016)
	$0.24K_D^{1.32}$	(25)	Powell and Uglow (1989)
	$-0.0135K_D^2 + 0.4959K_D - 0.0359$	(26)	Monaco et al. (2014)
V_s	$\frac{0.01V_s^2}{\sigma_v'}$	(27)	Long and L'Heureux (2022)
	$\frac{0.106V_s^{1.47}}{\sigma_v'}$	(28)	Mayne et al. (1988) as cited in Long and L'Heureux (2022)
	$\frac{0.007691V_s^{2.009}}{\sigma_v'}$	(29)	L'Heureux and Long (2017)
	$\frac{0.1097V_s^{1.3575}}{\sigma_v'}$	(30)	Duan et al. (2019)

Table 5
Selected methods for the constrained modulus (E_{oed}).

Workflow	Method		Author
CPT	$\alpha_M(q_t - \sigma_v);\ \alpha_M = Q_{tn};$ for $I_{cn} \geq 2.2$ & $Q_{tn} < 14$	(31)	Robertson (2009)
DMT	$R_M E_D;$ for $I_D < 0.6;\ R_M = 0.14 + 2.36\log K_D$	(32)	Marchetti (1980), Marchetti et al. (2001)
V_s	$0.00010V_s^{2.212}$ (E_{oed} in MPa)	(33)	L'Heureux and Long (2017)

Table 6
Selected methods for the shear wave velocity (V_s).

Workflow	Method		Author
CPT	$(10.1\log q_c - 11.4)^{1.67}(f_s/q_c \times 100)^{0.3}$	(34)	Hegazy and Mayne (1995)
	$3.18q_c^{0.549}f_s^{0.025}$	(35)	Hegazy and Mayne (1995)
	$[\alpha_{vs}(q_t - \sigma_v)/p_a]^{0.5};\ \alpha_{vs} = 10^{(0.55I_{cn}+1.68)}$	(36)	Robertson (2015)
	$1.75q_c^{0.627}$	(37)	Mayne and Rix (1995)
	$6.53(q_c - \sigma_v)^{0.461}$	(38)	Mayne and Rix (1995)
	$2.944q_t^{0.613}$	(39)	Long and Donohue (2010)
	$14.4(q_t - \sigma_v)^{0.265}(\sigma_v')^{0.137}$	(40)	Taboada et al. (2013)
	$7.95q_t^{0.403}$	(41)	Cai et al. (2014)
	$4.541q_t^{0.487}(1 + B_q)^{0.337}$	(42)	Cai et al. (2014)
	$8.35(q_t - \sigma_v)^{0.22}(\sigma_v')^{0.357}$	(43)	L'Heureux and Long (2017)

Table 7
Selected methods for the small-strain shear modulus (G_0).

Workflow	Method		Author
DMT	$7.5E_D$	(44)	as mentioned in Tanaka and Tanaka (1998)
	$26.177K_D^{-1.0066}M_{DMT}$; for $I_D < 0.6$	(45)	Marchetti et al. (2008)
V_s	ρV_s^2	(46)	

Table 8
Selected methods for the undrained shear strength (s_u).

Workflow	Method		Author
CPT	$\frac{q_t-\sigma_v}{N_{kt}}$; $N_{kt}=12$	(47)	Mayne (2016)
	$\frac{q_t-\sigma_v}{N_{kt}}$; $N_{kt}=10.5-4.6\ln(B_q+0.1)$	(48)	Mayne et al. (2023)
	$\frac{u_2-u_0}{N_{\Delta u}}$; $N_{\Delta u}=6$	(49)	Mayne (2016)
	$\frac{u_2-u_0}{N_{\Delta u}}$; $N_{\Delta u}=7.9+6.5\ln(B_q+0.3)$	(50)	Mayne et al. (2023)
	$\frac{q_t-u_2}{N_{ke}}$; $N_{ke}=8$	(51)	Mayne (2016)
	$\frac{q_t-u_2}{N_{ke}}$; $N_{ke}=4.5-10.66\ln(B_q+0.2)$	(52)	Mayne et al. (2023)
DMT	$0.12(P_0-\sigma_v)$	(53)	Cao et al. (2016)
	$0.09(P_1-\sigma_v)$	(54)	Cao et al. (2016)
	$0.22\sigma'_v(0.5K_D)^{1.25}$	(55)	Marchetti (1980)
	$0.018(E_D)$	(56)	Kamei and Iwasaki (1995)
	$0.35\sigma'_v(0.47K_D)^{1.14}$	(57)	Kamei and Iwasaki (1995)
V_s	$0.152V_s^{1.142}$	(58)	Agaiby and Mayne (2015)
	$0.021V_s^{1.52}$	(59)	L'Heureux and Long (2017)
	$0.016V_s^{1.50}$	(60)	Duan et al. (2019)

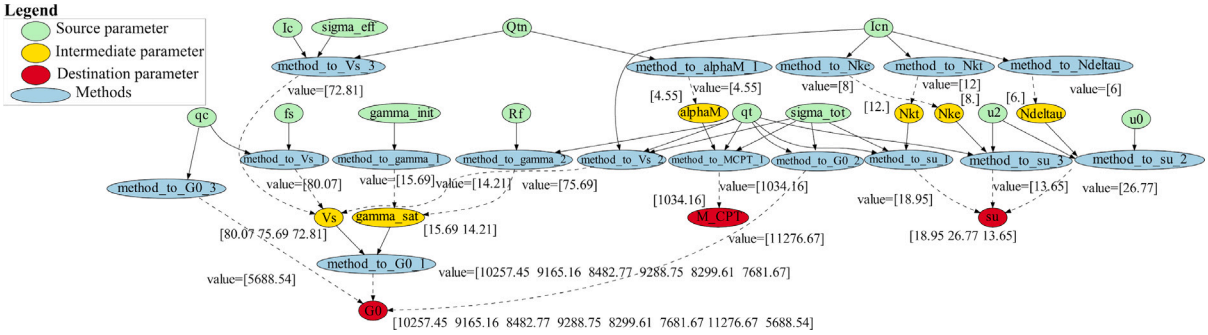

Fig. 8. Example of a generated graph for the CPT-based workflow.

process resulted in 18 layers for the CPTu, DMT, and V_s profiles. The APD system generated 18 graphs corresponding to the 18 layers. An example of such a graph is shown in Fig. 8.

The comparison between the output of APD (using the selected methods presented in the previous subsections) and the reference values interpreted at Onsøy soft clay test site is presented in Fig. 9. The blue, green, and red shaded areas represent the range of values obtained from the CPT, DMT, and V_s workflows, respectively. The blue, green, and red lines with circle markers correspond to the average value of the selected methods for the three workflows (CPT, DMT and V_s). The circle markers indicate the mid-depth of the 18 thin (1 m thick) layers.

The total unit weight was determined based on direct measurements (Gundersen et al., 2019). Fig. 9a presents the output of the three workflows using the methods illustrated in Table 3. Starting with the CPT-based workflow, as demonstrated by the upper bound of the range (blue shaded area), some methods accurately predicted the 'reference' values. However, since most CPT methods underestimated the measured unit weight, the average of the CPT-based workflow also underestimates the measured values. The average values of both the DMT and V_s based workflows agree reasonably well with the 'reference' values.

The evaluation of OCR was based on oedometer tests, either from incremental loading (IL) tests or from constant rate of strain (CRS) tests. The quality of the tested samples was determined according to Lunne et al. (1997a). Samples of quality class 1 and 2 are considered for the comparison as discussed in more detail in Gundersen et al. (2019), however in Fig. 9b all samples results were added irrespective of their sample quality as there were only two soil specimens of high quality (at area SEC where the selected in-situ tests were executed). Fig. 9b displays the results obtained from the methods listed in Table 4. The average of the three workflows indicates a slightly overconsolidated clay, which is consistent with the 'reference' values. However, some CPT and DMT methods tend to overpredict the OCR values.

Janbu modulus concept was used to determine the constrained modulus (Gundersen et al., 2019). Methods used to compute E_{oed} are presented in Table 5. Fig. 9c shows that the CPT-based workflow estimates are in good agreement with the 'reference' values, except for the last layer where E_{oed} is underestimated. The DMT-based workflow produces also a reliable estimate for E_{oed}, while the V_s-based workflow overestimates the 'reference' E_{oed} values (see red line in Fig. 9c).

Reference G_0 values were assessed using several seismic cone penetration tests (SCPTu 7, 8, 18 and 23 (ONSC 7, 8, 18 and 23) in the database uploaded to Datamap), and 1 SDMT. Table 7 displays the methods chosen for computing G_0, and Fig. 9d presents the results. Starting with the V_s-based workflow, the difference between the obtained values and the 'reference' values (SDMT in Fig. 9d) is attributed to the unit weight. Unit weights computed from Eqs. (14–17), were used in Eq. (46) to compute G_0. It is evident that the V_s-based workflow

produces the most reliable G_0 values as it uses measured V_s directly as an input. The DMT-based workflow significantly underestimates G_0. The 10 selected methods (Eqs. (34–43)) used to compute V_s in the CPT-based workflow result in a very wide range of G_0 values. However, for this particular case study, the average of this range shows good agreement with the 'reference' values.

The "reference" s_u values were obtained based on undrained anisotropically consolidated triaxial (CAUC) tests (Gundersen et al., 2019). Fig. 9e presents that obtained values for s_u based on the methods given in Table 8. The DMT-based workflow produces an overall reasonable agreement with the "reference" s_u values. The V_s based workflow overestimates the reference values in Unit II, although a reasonable agreement is obtained in Unit III. On average, the CPT-based workflow overestimates the reference s_u values. This highlights the importance of selecting appropriate bearing factors. N_{kt} varies from 10 to 18, while $N_{\Delta u}$ varies from 2 to 10 (Robertson, 2015). For a more conservative estimates of s_u, higher cone factors should be selected (Robertson, 2015).

5.1. Influence of the unit weight

As previously mentioned, the initial unit weight plays an important role in APD analysis. Since this unit weight is used to determine certain CPT and DMT parameters, such as Q_{tn}. These parameters act as source parameters in APD, specifically for the stratification in Module 2 (Section 2.2).

The impact of the initial unit weight on the results is examined using representative values for the four different units as the initial weight. These representative unit weights were determined using several methods (from water content, Multi-Sensor Core Logging (MSCL) and direct measurements) that compare reasonably well (Gundersen et al., 2019). For Units I, II, III and IV, representative unit weights of 17.5, 16.2, 17.8 and 16.2 kN/m^3 were selected, respectively (Gundersen et al., 2019).

The comparison was made using the same selected methods given in Tables 4, 5, 6, 7 and 8. The average of all methods for the four parameters (OCR, E_{oed}, G_0 and s_u) for the representative unit weights is compared with the results presented in the previous subsection. Note that the results in the previous subsection use Eq. (2) as the initial unit weight for the CPT and V_s-based workflows and Fig. 5 as the initial unit weight for the DMT-based workflow. It is clear that using different values for the initial unit weight would alter this comparison.

The results of this study are shown in Fig. 10. The average of the selected methods for the four parameters using the representative unit weights is indicated by the blue, green and red lines for the CPT, DMT and V_s workflows respectively (CPT_updated, DMT_updated and V_s_updated in Fig. 10). The results presented in the previous subsection are also shown in Fig. 10 using transparent colours (CPT, DMT and V_s in Fig. 10).

For the CPT-based workflow, using the representative unit weight as the initial unit weight would decrease the average value of OCR and E_{oed} (Figs. 10a-b) (compared to using Eq. (2) as the initial unit weight). The average value of G_0 would increase (Fig. 10c) and in the considered case study the effect on the average s_u is negligible (Fig. 10d). Regarding the DMT-based workflow, using the representative unit weight as the initial unit weight would decrease the average value of OCR, E_{oed} and s_u (Figs. 10a-b,d). However, the effect on the average G_0 is negligible (Fig. 10c). Concerning the V_s-based workflow, using the representative unit weight as the initial unit weight would decrease the average value of OCR (Fig. 10a) and would increase the average value of G_0 to match the 'reference' G_0 values (Fig. 10c).

The initial unit weight has an impact on a number of aspects of the APD from the early stages of the analysis onwards. It is therefore recommended to determine a representative value for the unit weight through relatively inexpensive tests that can be conducted at the early stages of the project. If such tests are not available, the values used for the initial unit weight should be compared with unit weights generally used at a particular site (experience). A method is currently being implemented to enable system users to rerun the analysis based on an updated initial unit weight obtained in module 4 of the different APD workflows.

5.2. Evaluating the uncertainty

Fig. 9 presents the values obtained from the three workflows. Additionally, the mean value of each based workflow is illustrated in the figure. In the context of uncertainty in soil properties, a number of factors must be taken into account. One such factor is the spatial variability, which can be evaluated through the use of random fields with statistical measures such as the mean and variance (Vanmarcke, 1977, 1983). In addition to the spatial variability, other considerations, including measurement uncertainty, statistical uncertainty and transformation uncertainty, also play a role in determining soil parameters (Phoon and Kulhawy, 1999a,b).

In APD, the parameters are evaluated based on indirect measurements (e.g. CPT, DMT and V_s) through a set of correlations (transformation models) provided by the users. In the graph-based approach, the values of a given parameter (represented by a node in the graph) are calculated using a number of paths, the number of which depends on the number of available correlations. An illustrative example of this graph is provided in Fig. 8. For each path, the mean and standard deviation are calculated. In order to consider the contributions of multiple distributions (arising from disparate paths in the graph) into a unified distribution, it is necessary to assess the combined mean and variance. The combined mean is calculated as a weighted average of the means of each contributing path, while the combined variance can be calculated using the method proposed by Dormann et al. (2018). Nevertheless, the existence of multiple paths to each parameter presents a significant challenge in the implementation of these approaches to assess the uncertainty in the derived values. Consequently, the mean of all values can be considered as the representative value for a parameter as a preliminary estimate in the initial stages of the project.

Fig. 11 provides insight into the uncertainty, as reflected in the statistical measures. The results for the five parameters (γ_t, OCR, E_{oed}, G_0 and s_u) are presented in Figs. 11a-e, respectively. For each layer (18 layers in total), the values computed from the three workflows (CPT, DMT and V_s) are collated. For example, 13 values are collected for γ_t (4 from the CPT-based workflow, 5 from the DMT-based workflow and 4 from the V_s-based workflow). Subsequently, the mean, median and standard deviation are calculated. For each parameter at each layer, a confidence interval is plotted. In Fig. 11, the 95% confidence interval for the mean values of the different parameters is calculated in order to provide an estimate of the uncertainty associated with the values. The confidence interval provides an estimate of the range within which the true mean of the population is expected to lie, given a specified level of confidence, here 95%. The calculation of the confidence intervals is based on the standard error of the mean and the critical value from the t-distribution, which is specific to the given confidence level. In each confidence interval, the median is indicated by a blue circle, while the mean is represented by a black circle. The standard deviation (σ) is illustrated by the grey dotted line, with the corresponding values presented on the top x-axis. Additionally, the figure includes the reference values for each parameter for comparison purposes.

A comparison of Figs. 9 and 11 demonstrates that the scatter in the obtained values for unit weight (from CPT, DMT and V_s) is not consistent with depth. With regard to OCR, the scatter is the highest in the upper layers, then it decreases to a nearly constant value with depth. In the case of the constrained modulus, only three values were computed for each depth (Table 5). As a result of the higher values obtained from the V_s-based workflow in comparison to those obtained from CPT and DMT-based workflows, the scatter is quite high. For both G_0 and s_u, the scatter increases with depth.

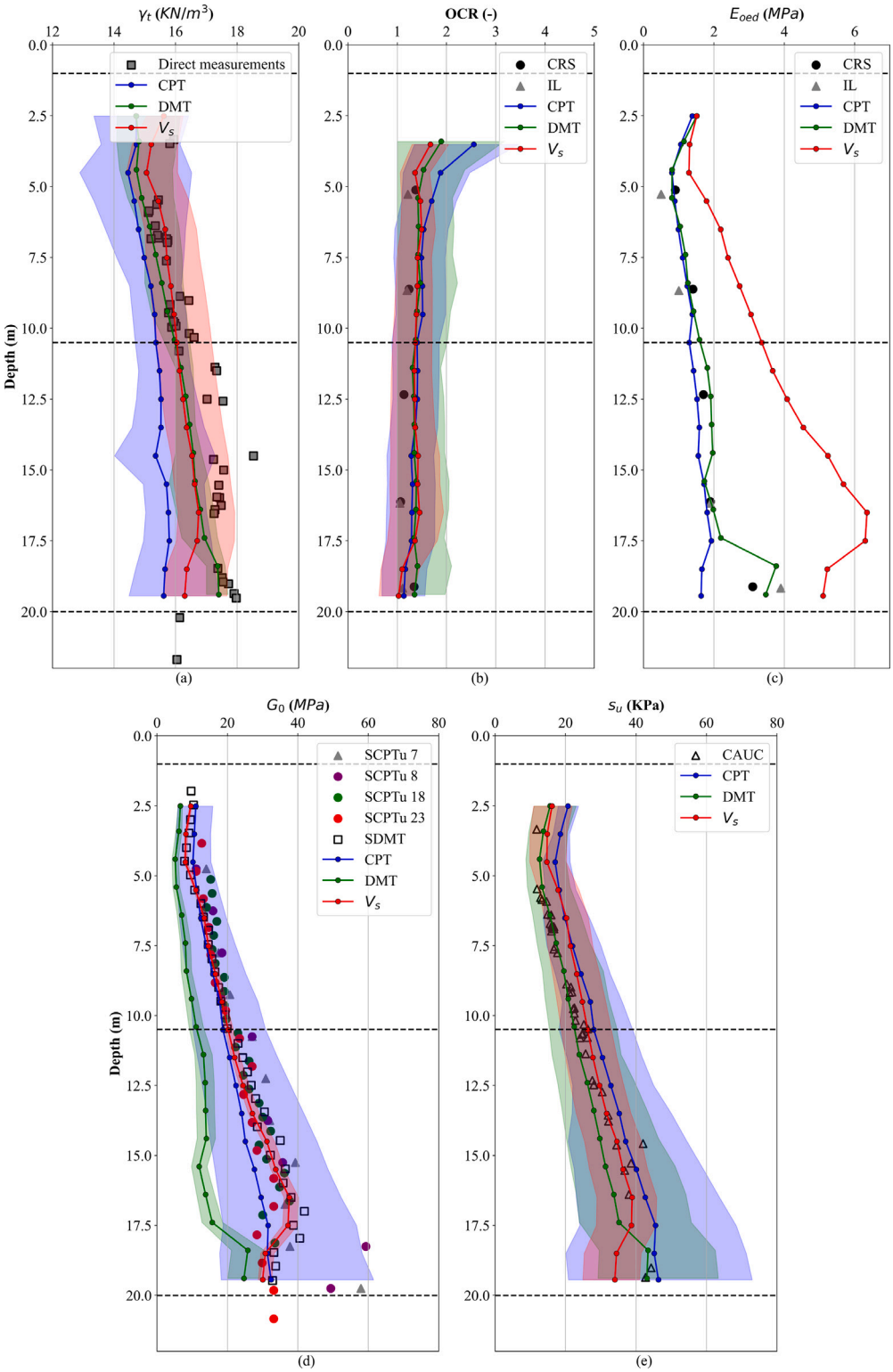

Fig. 9. Comparison between APD and interpreted values at Onsøy soft clay test site (the blue, green, and red shaded areas represent the range of values obtained from the CPT, DMT, and V_s workflows, respectively).

5.3. Additional studies

The parameters presented in Fig. 9 have been evaluated based on one CPTu (CPTu 18), one SDMT and one V_s profile obtained from the SDMT. This subsection presents a comprehensive comparison utilizing multiple in-situ tests to assess the reproducibility of the results and to investigate the uncertainty. In this study, 13 CPTu from zone SEC (see Fig. 6) and the V_s profile from four SCPTu were employed. As only one DMT was available at the test site, it was not considered in this analysis. The results of the 13 CPTu and the V_s profiles are presented in Fig. 12. The V_s profile for the SCPTu was obtained by combining the four V_s profiles from the four SCPTu, as some SCPTu had few V_s measurements. It was therefore decided to combine the four profiles into one. The 13 selected CPTu are CPTu 7, 8, 9, 10, 16, 17, 18, 22,

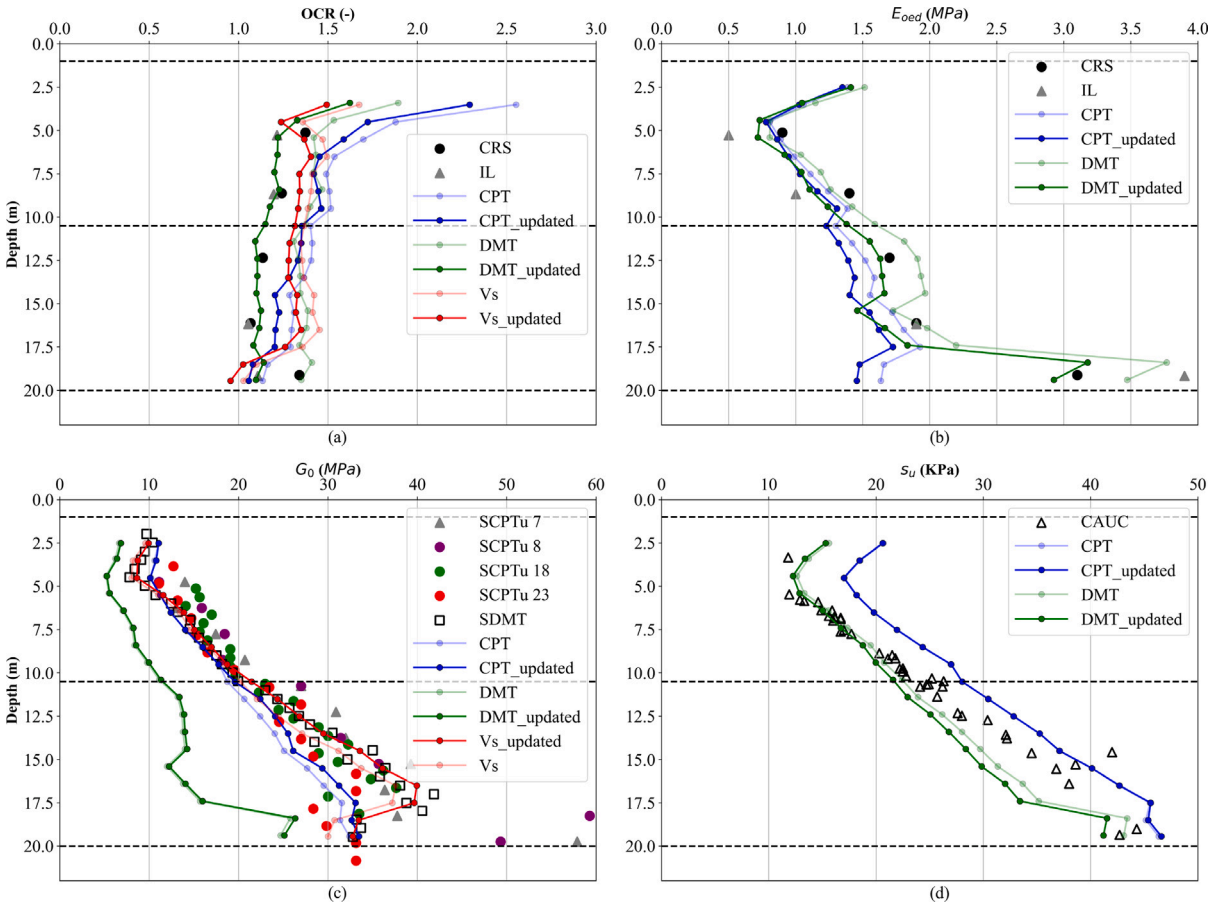

Fig. 10. Influence of the initial unit weight on the results.

23, 25, 26, 27 and 28. The results of CPTu 18 (which was used for the CPT-based workflow in Fig. 9) are plotted in black in Fig. 12. The same methods (presented in Tables 3, 4, 5, 6, 7 and 8) were used.

Fig. 13 presents the results obtained from the CPT (using the 13 tests shown in Fig. 12) and V_s-based workflows (using the 2 V_s profiles shown in Fig. 12). It should be noted that the shaded areas plotted in Fig. 13 have been calculated in a different manner to those highlighted in Fig. 9. In the current analysis, the shaded area represents the average of all the tests. To illustrate, in the case of the unit weight for the CPT-based workflow (Fig. 13a), the average of the four methods (presented in Table 3) is initially calculated for each CPT. Consequently, for each of the 18 layers, there will be 13 averages obtained from the 13 CPTs (see Fig. 12). The lower bound of the shaded area in Fig. 13a represents the minimum of the 13 averages, while the upper bound of the shaded area represents the maximum of the 13 averages. The blue line with circle markers presents the average of the 13 averages. Therefore, the results presented in Fig. 13 are quite different from those shown in Fig. 9. In Fig. 9, the lower bound showed the minimum value obtained from the selected methods, while the upper bound presented the maximum value obtained from the methods. Similarly, the same representation is employed for the V_s-based workflow and for the other parameters.

A comparison of Fig. 13 with Fig. 9 demonstrates that the computed average remained relatively consistent when additional V_s profiles and additional CPTu soundings were employed. This was observed for both γ_t and OCR. In the case of the CPT-based workflow, the incorporation of supplementary CPTu soundings resulted in a reduction in the mean values for E_{oed}, G_0 and s_u. In contrast, the additional V_s profiles introduced into the V_s-based workflow resulted in a slight variation in the average values for E_{oed}, G_0 and s_u.

As with Fig. 11, Fig. 14 offers insight into the uncertainty, as reflected in the statistical measures. Additionally, Fig. 14 includes the results of the DMT-based workflow. To illustrate, Fig. 14a presents the results for the unit weight across all layers. A total of 65 values are considered, comprising 52 values derived from the CPT-based workflow (13 CPTu soundings, 4 values for each), 5 values from the DMT-based workflow, and 8 values from the V_s-based workflow (2 V_s profiles, 4 values each). The same observations made regarding Fig. 11 are also applicable to Fig. 14. It can be seen that the scatter in the obtained values for unit weight is not consistent with depth. With regard to OCR, the scatter is the highest in the upper layers, then it decreases to a nearly constant value with depth. For E_{oed}, G_0 and s_u, the scatter increases with depth.

This subsection presents an analysis in which additional sources for the CPT and V_s-based workflows were employed to evaluate γ_t, OCR, E_{oed}, G_0 and s_u. An increase in the number of sources would, to some extent, result in an elevated level of scatter (and uncertainty) in the derived values for the parameters. Nevertheless, the results demonstrate that it is still feasible to derive reasonable predictions for the parameters, which is a valuable contribution, particularly in the initial stages of a project.

6. Connection between soil parameters and numerical analysis

The main aim of APD is to create material sets that can be used directly for numerical analysis. This section illustrates the connection between APD and a finite element software (PLAXIS). The connection requires two main elements; stratification and constitutive model parameters. The stratification in this case is determined in module 2 by one of the three approaches briefly discussed in Section 2.2. Constitutive model parameters are assessed based on the methods

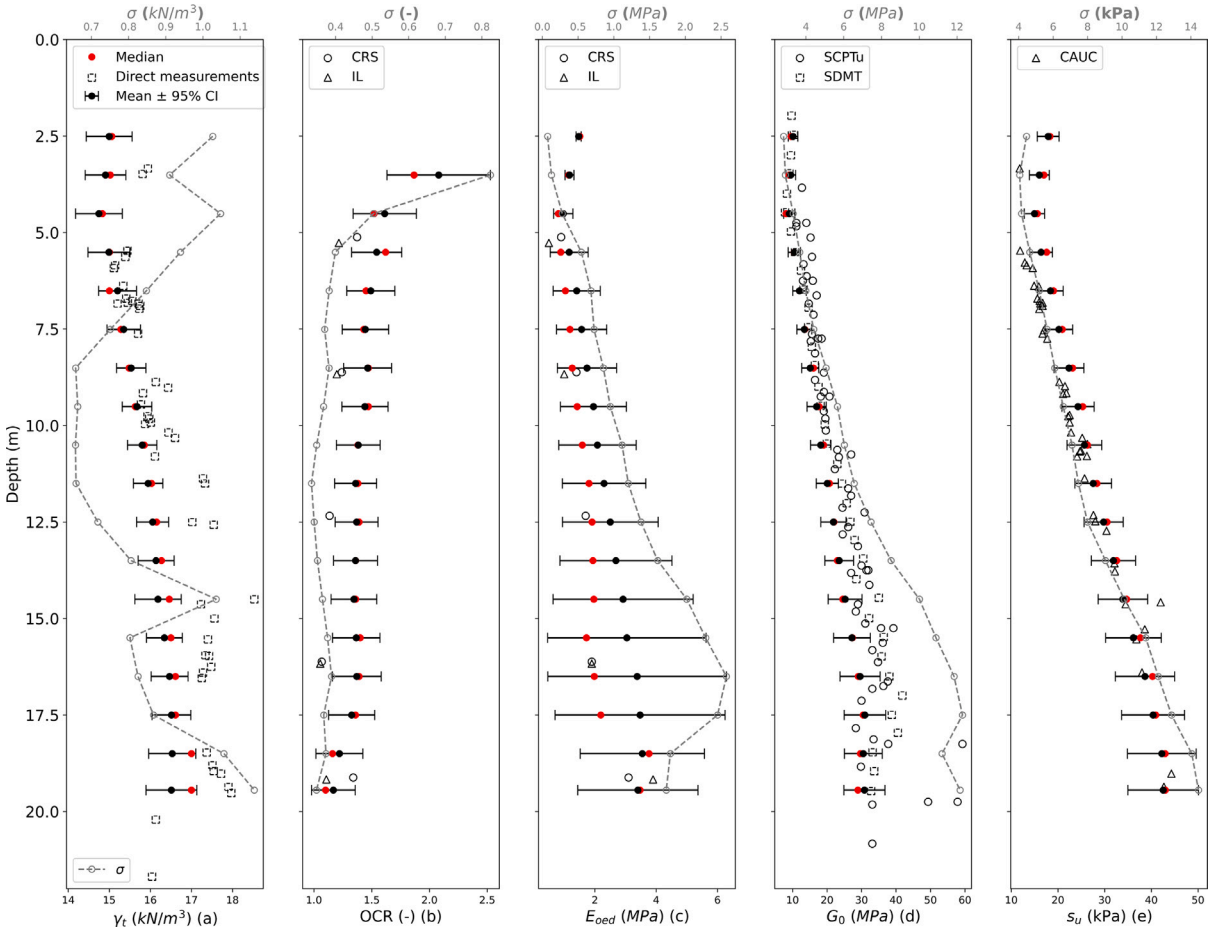

Fig. 11. Scatter in the obtained values represented by confidence intervals and standard deviation.

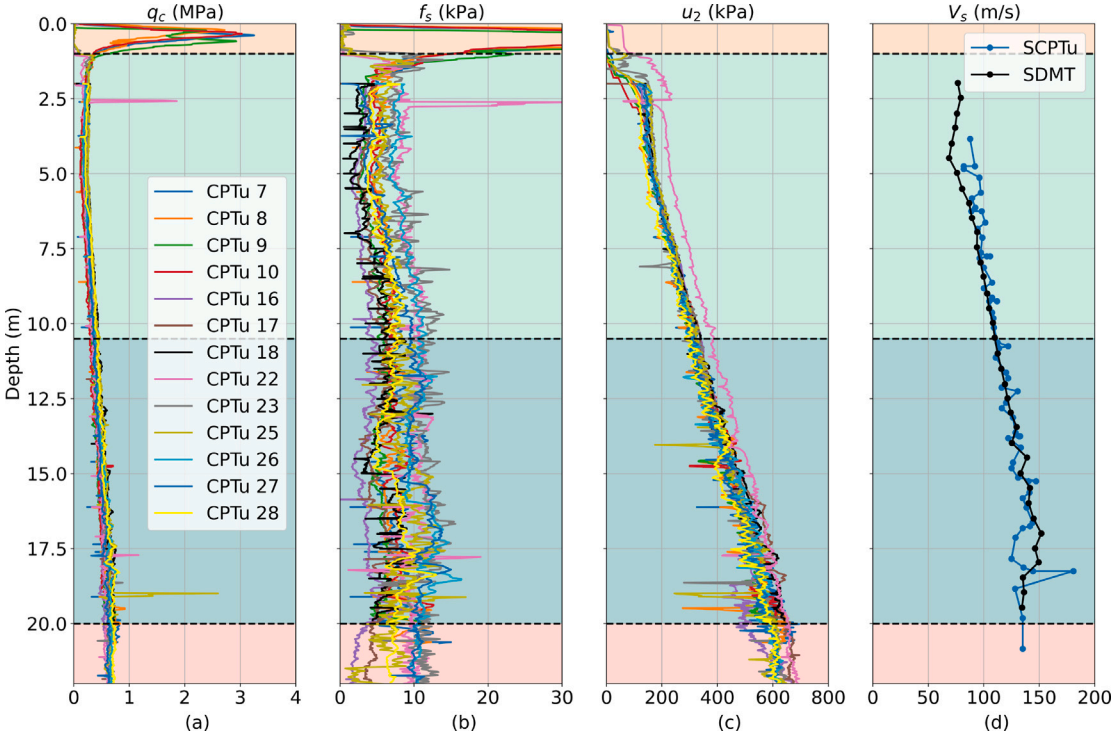

Fig. 12. Results of selected in-situ tests, (a–c): CPTu results (profiles of q_c, f_s and u_2); (d): V_s profile from the SDMT.

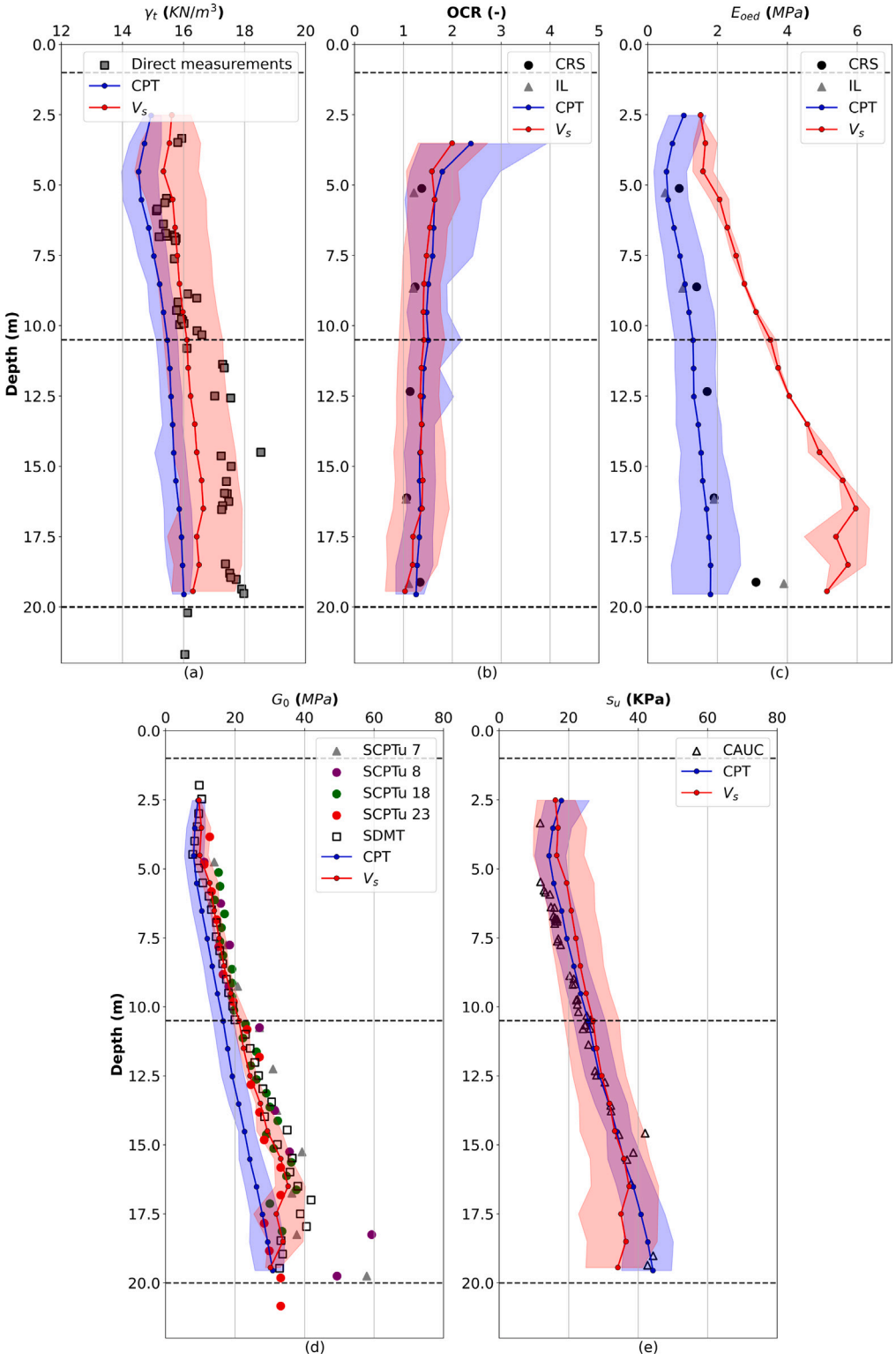

Fig. 13. Comparison between APD and interpreted values at Onsøy soft clay test site (the blue and red shaded areas represent the range of values obtained from the CPT and V_s workflows, respectively).

provided by the user (as explained in Section 2.4.3). The choice of constitutive model is not constrained by any limitations. It is possible for users to select any constitutive model, provided that the parameters can be evaluated. In principle, the soil properties and soil parameters are initially determined. Subsequently, a constitutive model is selected, which may be any model deemed appropriate for the soil type in consideration. The constitutive model parameters are then determined based on the soil properties and soil parameters.

The test site described in Section 4.1 is used as an illustrative example for verifying the implementation of the linkage between APD and the finite element software. It is not the intention of this section to investigate the optimal constitutive model for this particular type of

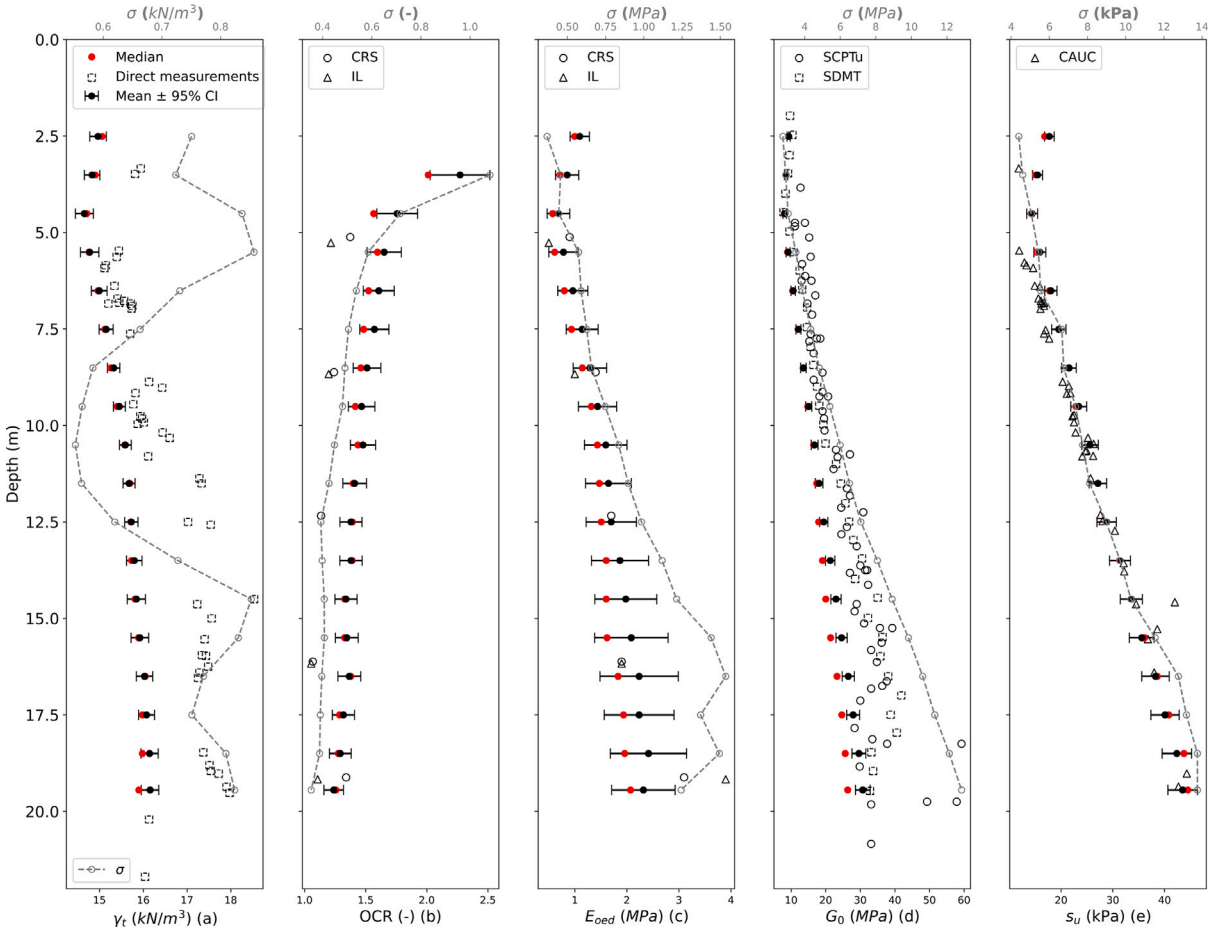

Fig. 14. Scatter in the obtained values represented by confidence intervals and standard deviation.

soil or to verify the obtained material set through numerical analysis. The objective is to determine the parameters for the Modified Cam Clay model using the CPT-based workflow to demonstrate the potential of APD.

6.1. Modified Cam Clay model

The Modified Cam Clay (MCC) model is an elastic–plastic model based on critical state soil mechanics. It assumes a logarithmic relationship between the mean effective stress and the void ratio. The model is described in more detail in several publications, such as Muir Wood (1990).

The parameters required for the MCC model are as follows:

- Cam-Clay compression index λ
- Cam-Clay swelling index κ
- Poisson's ratio ν_{ur}
- Void ratio e_0
- Tangent of the critical state line M

The compression index (C_c) and swelling index (C_s) are used to determine the Cam-Clay compression and swelling indices, respectively as follows:

$$\lambda = \frac{C_c}{2.3} \tag{61}$$

$$\kappa \approx \frac{C_s}{2.3} \tag{62}$$

C_s can be estimated from C_c as suggested by Lengkeek (2022):

$$C_s = 0.16 C_c \tag{63}$$

In literature, there are several correlations between the compression index (C_c) and various index parameters, such as the plasticity index (PI), liquid limit (LL), water content (w_0), and void ratio (e_0). The APD database contains 49 methods for determining C_c using various index parameters. For this study, 19 methods were selected to determine C_c, as shown in Table A.11. These 19 methods are all the methods in the database that depend on either the plasticity index or the void ratio, while one method depends on the friction ratio (R_f).

The plasticity index can be calculated from the CPT measurements using the method described by Ramsey and Tho (2022):

$$PI = \frac{17.5 R_f (1 + B_q)^{1.2}}{(0.33 Q_t)^{0.31}} \tag{64}$$

When the soil is fully saturated, the saturated unit weight of soil can be determined as follows:

$$\gamma_{sat} = \frac{(G_s + e_0)\gamma_w}{1 + e_0} \tag{65}$$

Eq. (65) can be rewritten to determine the void ratio from the saturated unit weight:

$$e_0 = \frac{\gamma_{sat} - G_s \gamma_w}{\gamma_w - \gamma_{sat}} \tag{66}$$

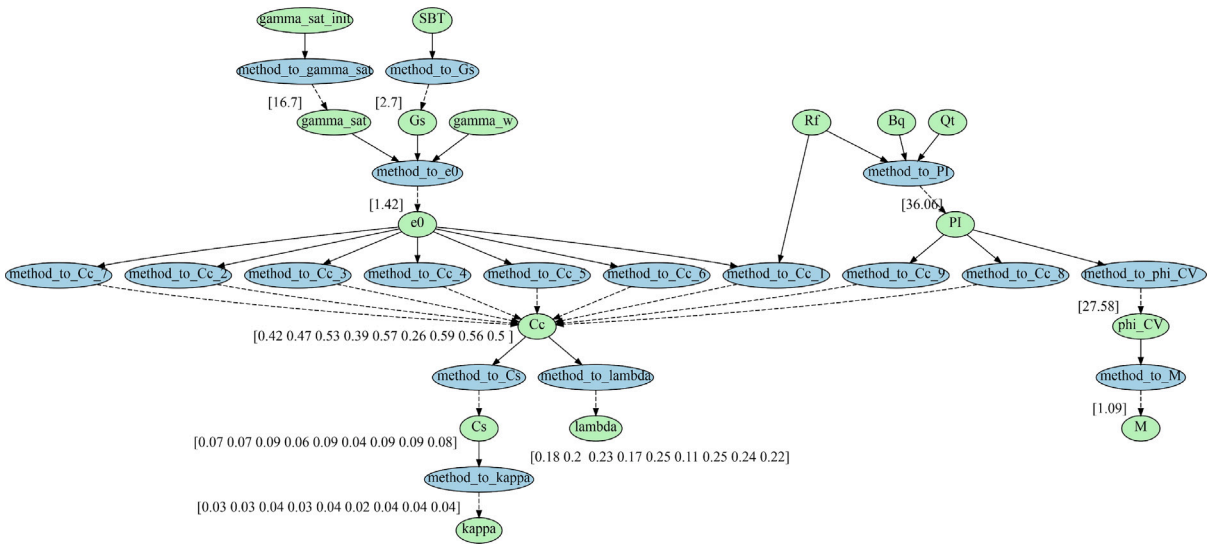

Fig. 15. Graph for layer 11.

The tangent of the critical state line M is determined based on the effective friction angle as follows:

$$M = \frac{6 \sin \varphi'}{3 - \sin \varphi'} \tag{67}$$

Within the framework of Critical State Soil Mechanics (CSSM) it is necessary to use the critical state friction angle (φ'_{cv}) rather than the peak friction angle (φ'_p). The normally consolidated earth pressure coefficient K_0^{nc} is assumed to be based on Jaky's empirical formula (Jaky, 1944) and the critical state friction angle (Mesri and Hayat, 1993). The method proposed by Mitchell (1976), cited in Kulhawy and Mayne (1990), can be used to obtain the critical state friction angle for clays as follows:

$$\sin \varphi'_{cv} = 0.8 - 0.094 \ln PI \tag{68}$$

6.2. Proof of concept

The aim of this section is to present the fully automated workflow of APD and to outline the process of converting field test data into soil layer geometry, determining soil and constitutive model parameters, and connecting them to a finite element software for numerical analysis. The CPTu results, illustrated in Fig. 7a-c, represent the used field test data. The stratification follows the same averaging approach (manual stratification) presented in the previous section, resulting in 18 layers. As previously noted, alternative stratification approaches may be employed. In the case of more complex and refined stratification (for example, 3D stratification), alternative approaches may be employed, as illustrated by Brinkgreve et al. (2023, 2024). Soil and constitutive model parameters are determined based on the Methods CSV file shown in Table A.11.

The APD system automatically establishes a connection to the finite element software. A borehole consisting of 18 layers was created, and the corresponding material sets were defined. The graph for layer 11 is shown exemplary in Fig. 15 (note: only 9 out of the 19 methods used to compute C_c are displayed in the graph for visualization purposes). The specific gravity (G_s in the graph) was set to 2.7, and the unit weight of water (gamma_w in the graph) was set to 10 kN/m^3. The initial unit weight (gamma_sat_init in the graph) was computed using Eq. (2). The values for the source parameters for this graph are shown in Table 9. The resulting material set for this layer is the average of all computed values for different parameters and is presented in Table 10.

Table 9
Source parameters for layer 11.

Parameter	Value
gamma_sat_init (kN/m^3)	16.7
SBT (–)	3
R_f (%)	1.165
B_q (–)	0.75
Q_t (–)	4.21

Table 10
MCC material set for layer 11.

Parameter	Value
γ_{sat} (kN/m^3)	16.7
λ (–)	0.2026
κ (–)	0.03316
ν'_{ur} (–)	0.15
e_{init} (–)	1.421
M (–)	1.09

6.3. Comments related to module 5

This section presents a proof of concept highlighting the transition between soil parameters to constitutive model parameters. Moreover, the automatic and direct connection between APD to the finite element software was presented. For this study, the parameters were determined for the MCC model. Nevertheless, the APD database also includes methods for other constitutive models, such as the Hardening Soil model (Schanz et al., 1999) and the Hardening Soil model with small-strain stiffness (HSsmall) (Benz, 2007).

Validating the output of module 5 can be achieved by simulating soil tests (oedometer tests) using a single point algorithm (SoilTest Tool) to investigate stress–strain behaviour and to compare the results with available oedometer tests at the site. Additionally, the entire numerical model can be validated by modelling a one-dimensional compression of a soil column. The validation process is part of ongoing research.

7. Conclusions and next steps

This paper introduces an automatic parameter determination (APD) framework, which utilizes a graph-based approach to assess parameters from in-situ tests. This is particularly useful during the early

Table A.11
Methods CSV file containing selected methods used for analysis in Section 6.

Method_to	Formula	Parameters_in	Parameters_out	Validity	Reference[a]
method_to_PI	17.5*Rf*(1+Bq)**1.2/(0.33*Qt)**0.31	Rf,Bq,Qt	PI	SBT(234)	Ramsey_2022
method_to_M	(6*sin(radians(phi_CV)))/(3-sin(radians(phi_CV)))	phi_CV	M	SBT(123456789)	
method_to_e0	((gamma_sat)-Gs*gamma_w)/(gamma_w-(gamma_sat))	gamma_sat,Gs,gamma_w	e0	SBT(123456789)	Analytical
method_to_phi_CV	degrees(arcsin(0.8-0.094*log(PI)))	PI	phi_CV	SBT(234)	Kulhawy&Mayne_1990
method_to_Cc_1	(0.036*Rf+0.132)*(1+e0)	Rf,e0	Cc	SBT(234)	Lengkeek_2022
method_to_Cc_2	0.4*(e0-0.25)	e0	Cc	SBT(234)	Azzouz_1976
method_to_Cc_3	0.62*(e0-0.56)	e0	Cc	SBT(234)	Kogure_1977
method_to_Cc_4	0.42*(e0-0.5)	e0	Cc	SBT(234)	Abdrabbo_1990
method_to_Cc_5	0.54*(e0-0.37)	e0	Cc	SBT(234)	Yoon_2004
method_to_Cc_6	0.2875*(e0-0.5082)	e0	Cc	SBT(234)	Vinod_2010
method_to_Cc_7	(0.49*e0)-0.11	e0	Cc	SBT(234)	Park_2011
method_to_Cc_8	0.014*(PI+3.6)	PI	Cc	SBT(234)	Sridharan_Nagaraj_2000
method_to_Cc_9	0.014*PI	PI	Cc	SBT(234)	Tiwari_2012
method_to_Cc_10	(0.286*e0)-0.054	e0	Cc	SBT(234)	Abbasi_2012
method_to_Cc_11	0.3921*e0	e0	Cc	SBT(234)	Tiwari_2012
method_to_Cc_12	(0.3608*e0)-0.0713	e0	Cc	SBT(234)	Kalantary_2012
method_to_Cc_13	exp((1.272*log(e0))-1.282)	e0	Cc	SBT(234)	Lav_2001
method_to_Cc_14	0.54*(e0-0.35)	e0	Cc	SBT(234)	Nishida_1956[b]
method_to_Cc_15	0.35*(e0-0.5)	e0	Cc	SBT(234)	Hough_1957[c]
method_to_Cc_16	0.43*(e0-0.25)	e0	Cc	SBT(234)	Cozzolino_1961[b]
method_to_Cc_17	0.02 + 0.014*PI	PI	Cc	SBT(234)	Nacci_1975[b]
method_to_Cc_18	0.046 + 0.0104*PI	PI	Cc	SBT(234)	Nakase_1988
method_to_Cc_19	0.5*Gs*(PI/100)	PI,Gs	Cc	SBT(234)	Wroth&Wood_1978
method_to_Cs	0.160*Cc	Cc	Cs	SBT(234)	Lengkeek_2022
method_to_lambda	Cc/2.3	Cc	lambda	SBT(234)	
method_to_kappa	Cs/2.3	Cs	kappa	SBT(234)	

[a] Further Reading.
[b] as cited in Yoon et al. (2004).
[c] as cited in Sridharan and Nagaraj (2000).

phases of projects when soil data is limited. During this phase, cost-effective field tests such as CPT and DMT precede full laboratory testing. Nevertheless, employing APD during the project's early design stage enables users to gain more comprehensive insights efficiently. It is not the aim of the project to replace laboratory testing, but rather to complement it. Laboratory testing remains essential to refine soil and constitutive model parameters for final design. APD has two key attributes: transparency and adaptability. This allows users to enrich the system by incorporating their knowledge and experience, thus expanding the existing database of methods and parameters provided by the system.

Section 5 presented the derivation of soil parameters from the three workflows of the system (CPT, DMT and V_s). The results of several methods were compared with reference values interpreted from the results of laboratory tests conducted at Onsøy soft clay test site (NGTS). Such analysis helps to validate individual methods and to update/improve the compiled methods database. The results are presented based on the lower and upper bounds, as well as the average, for the three workflows. Using the average as a representative value for different parameters is questionable as it might take into account inaccurate methods. This is currently the biggest challenge due to the large number of methods within APD and the wide scatter of values obtained for the same parameters. A statistical module is being developed to assist in selecting the representative value.

Section 6 demonstrates the connection between APD and the finite element software. This is the central focus of the research project, as the primary objective is to use in-situ test results to determine constitutive model parameters and connect them directly to the numerical analysis. Parameters for the MCC model were assessed based on CPTu results employing the CPT-based workflow. As module 5 (where the transition between soil parameters to constitutive model parameters takes place) is still under development, the intention of this section was not to determine the optimal constitutive model for this particular soil type (Onsøy soft clay) or to validate the obtained material set against laboratory tests. The sole goal of this section is to demonstrate the connection between raw measurement data and APD, as well as the connection between APD and the finite element analysis. This should highlight the big potential of APD. Current research involves analysing additional test sites, expanding the system with more in-situ tests, and validating the output for soil and constitutive model parameters.

CRediT authorship contribution statement

Islam Marzouk: Writing – original draft, Visualization, Validation, Methodology, Investigation, Formal analysis, Conceptualization. **Ronald Brinkgreve:** Writing – review & editing, Project administration, Methodology, Conceptualization. **Arny Lengkeek:** Writing – review & editing, Project administration, Methodology, Conceptualization. **Franz Tschuchnigg:** Writing – review & editing, Supervision, Project administration, Methodology, Conceptualization.

Declaration of competing interest

The authors declare that they have no known competing financial interests or personal relationships that could have appeared to influence the work reported in this paper.

Data availability

The data used is open access and the web link to the data is mentioned in the paper.

Appendix. Methods CSV file used for Section 6 analysis

See Table A.11.

References

Agaiby, S.S., Mayne, P.W., 2015. Relationship between undrained shear strength and shear wave velocity for clays. In: Deformation Characteristics of Geomaterials. IOS Press, pp. 358–365. http://dx.doi.org/10.3233/978-1-61499-601-9-358.
Benz, T., 2007. Small-Strain Stiffness of Soils and Its Numerical Consequences (Ph.D. thesis). University of Stuttgart, Germany.
Brinkgreve, R.B.J., 2019. Automated model and parameter selection: Incorporating expert input into geotechnical analyses. GEOSTRATA Mag. 23 (1), 38–45. http://dx.doi.org/10.1061/geosek.0000115.

Brinkgreve, R.B.J., Engin, E., Engin, H.K., 2010. Validation of empirical formulas to derive model parameters for sands. In: Proceedings of the 7th NUMGE 2010, Trodheim, Norway.

Brinkgreve, R.B.J., Tschuchnigg, F., Laera, A., Brasile, R.S., 2023. Automated CPT interpretation and modelling in a BIM/Digital twin environment. In: Proceedings of the 10th European Conference on Numerical Methods in Geotechnical Engineering (NUMGE 2023), London. http://dx.doi.org/10.53243/NUMGE2023-111.

Brinkgreve, R.B.J., Zekri, A., Laera, A., 2024. Towards an integrated and automated digital workflow in geotechnical engineering. In: 7th International Conference on Geotechnical and Geophysical Site Characterization. ISC7, CIMNE, http://dx.doi.org/10.23967/isc.2024.153.

Burns, S., Mayne, P.W., 1996. Small- and high-strain measurements of in situ soil properties using the seismic cone penetrometer. Transp. Res. Rec.: J. Transp. Res. Board 1548, 81–88. http://dx.doi.org/10.3141/1548-12.

Cai, G., Puppala, A.J., Liu, S., 2014. Characterization on the correlation between shear wave velocity and piezocone tip resistance of jiangsu clays. Eng. Geol. 171, 96–103. http://dx.doi.org/10.1016/j.enggeo.2013.12.012.

Cao, L.F., Peaker, S.M., Ahmad, S., 2016. Use of flat dilatometer in ontario. In: Proceedigs of the Fifth International Conference on Geotechnical and Geophysical Site Characterisation, Gold Coast, Queensland, Australia. pp. 755–760.

Chakraborty, A., Dutta, T., Mondal, S., Nath, A., 2018. Application of graph theory in social media. Int. J. Comput. Sci. Eng. 6 (10), 722–729. http://dx.doi.org/10.26438/ijcse/v6i10.722729.

Clarke, B.G., 2022. Pressuremeters in Geotechnical Design, second ed. CRC Press, Boca Raton.

D'Ignazio, M., Lunne, T., Andersen, K.H., Yang, S., Di Buò, B., Länsivaara, T., 2019. Estimation of preconsolidation stress of clays from piezocone by means of high-quality calibration data. AIMS Geosci. 5 (2), 104–116. http://dx.doi.org/10.3934/geosci.2019.2.104.

Dijkstra, E.W., 1959. A note on two problems in connexion with graphs. Numer. Math. 1 (1), 269–271. http://dx.doi.org/10.1007/BF01386390.

Doherty, J.P., Gourvenec, S., Gaone, F.M., Pineda, J.A., Kelly, R., O'Loughlin, C.D., Cassidy, M.J., Sloan, S.W., 2018. A novel web based application for storing, managing and sharing geotechnical data, illustrated using the national soft soil field testing facility in Ballina, Australia. Comput. Geotech. 93, 3–8. http://dx.doi.org/10.1016/j.compgeo.2017.05.007.

Dormann, C.F., Calabrese, J.M., Guillera-Arroita, G., Matechou, E., Bahn, V., Bartoń, K., Beale, C.M., Ciuti, S., Elith, J., Gerstner, K., Guelat, J., Keil, P., Lahoz-Monfort, J.J., Pollock, L.J., Reineking, B., Roberts, D.R., Schröder, B., Thuiller, W., Warton, D.I., Wintle, B.A., Wood, S.N., Wüest, R.O., Hartig, F., 2018. Model averaging in ecology: A review of Bayesian, information–theoretic, and tactical approaches for predictive inference. Ecol. Monograph. 88 (4), 485–504. http://dx.doi.org/10.1002/ecm.1309.

Duan, W., Cai, G., Liu, S., Puppala, A.J., 2019. Correlations between shear wave velocity and geotechnical parameters for jiangsu clays of China. Pure Appl. Geophys. 176 (2), 669–684. http://dx.doi.org/10.1007/s00024-018-2011-x.

Felić, H., Peterstorfer, T., Marzouk, I., Tschuchnigg, F., 2024. Data-driven site characterization - focus on small-strain stiffness. In: 7th International Conference on Geotechnical and Geophysical Site Characterization. ISC7, CIMNE, http://dx.doi.org/10.23967/isc.2024.148.

Gansner, E., 2011. Drawing Graph with Graphviz. AT&T Bell Laboratories.

Gundersen, A.S., Hansen, R.C., Lunne, T., L'Heureux, J.S., Strandvik, S.O., 2019. Characterization and engineering properties of the NGTS Onsøy soft clay site. AIMS Geosci. 5 (3), 665–703. http://dx.doi.org/10.3934/geosci.2019.3.665.

Hegazy, Y.A., Mayne, P.W., 1995. Statistical correlations between vs and CPT data for different soil types.

Jaky, J., 1944. The coefficient of earth pressure at rest. J. Soc. Hung. Archit. Eng. 355–358.

Kamei, T., Iwasaki, K., 1995. Evaluation of undrained shear strength of cohesive soils using a flat dilatometer. Soils Found. 35 (2), 111–116. http://dx.doi.org/10.3208/sandf1972.35.2_111.

Kulhawy, F.H., Mayne, P.W., 1990. Manual on estimating soil properties for foundation design.

Lengkeek, H.J., 2022. Testing and Modeling of Sheet Pile Reinforced Dikes on Organic Soils: Insights from the Eemdijk Full-Scale Failure Test. Delft University of Technology, http://dx.doi.org/10.4233/uuid:78df5e2b-740e-4268-a821-ed0ccaae93e5.

Lengkeek, H.J., Brinkgreve, R.B.J., 2022. CPT-based unit weight estimation extended to soft organic clays and peat: An update. In: Cone Penetration Testing 2022. pp. 503–508. http://dx.doi.org/10.1201/9781003308829-71.

L'Heureux, J.S., Long, M., 2017. Relationship between shear-wave velocity and geotechnical parameters for norwegian clays. J. Geotech. Geoenviron. Eng. 143 (6), 04017013. http://dx.doi.org/10.1061/(ASCE)GT.1943-5606.0001645.

L'Heureux, J.S., Lunne, T., 2020. Characterization and engineering properties of natural soils used for geotesting. AIMS Geosci. 6 (1), 35–53. http://dx.doi.org/10.3934/geosci.2020004.

Likaj, R., Shala, A., Mehmetaj, M., Hyseni, P., Bajrami, X., 2013. Application of graph theory to find optimal paths for the transportation problem. IFAC Proc. Vol. 46 (8), 235–240. http://dx.doi.org/10.3182/20130606-3-XK-4037.00031, 15th IFAC Workshop on International Stability, Technology, and Culture.

Long, M., Donohue, S., 2010. Characterization of norwegian marine clays with combined shear wave velocity and piezocone cone penetration test (CPTU) data. Can. Geotech. J. 47 (7), 709–718. http://dx.doi.org/10.1139/T09-133.

Long, M., L'Heureux, J.S., 2022. Shear wave velocity—SCPTU correlations for sensitive marine clays. In: Gottardi, G., Tonni, L. (Eds.), Cone Penetration Testing 2022. CRC Press, pp. 515–520. http://dx.doi.org/10.1201/9781003308829-73.

Lunne, T., Berre, T., Strandvik, S., 1997a. Sample disturbance effects in soft low plastic norwegian clay. In: Symposium on Recent Developments in Soil and Pavement Mechanics, Rio de Janeiro, Brazil.

Lunne, T., Christoffersen, H.P., 1983. Interpretation of cone penetrometer data for offshore sands. In: Offshore Technology Conference. http://dx.doi.org/10.4043/4464-MS.

Lunne, T., Robertson, P.K., Powell, J.J.M., 1997b. Cone Penetration Testing in Geotechnical Practice, First edition CRC Press, Boca Raton, FL.

Mair, R.J., Wood, D.M., 1987. Pressuremeter Testing: Methods and Interpretation. Elsevier Science, Kent.

Marchetti, S., 1980. In situ tests by flat dilatometer. J. Geotech. Eng. Div. 106 (3), 299–321. http://dx.doi.org/10.1061/AJGEB6.0000934.

Marchetti, S., Crapps, D.K., 1981. Flat dilatometer manual, Internal Report of G.P.E. Inc.

Marchetti, S., Monaco, P., Totani, G., Calabrese, M., 2001. The Flat Dilatometer Test (DMT) in Soil Investigations – A Report by the ISSMGE Committee TC16.

Marchetti, S., Monaco, P., Totani, G., Marchetti, D., 2008. In situ tests by seismic dilatometer (SDMT). In: Proceedings of ASCE Geotechnical Special Publication honoring Dr. John H. Schmertmann: From research to practice in geotechnical engineering. pp. 292–311. http://dx.doi.org/10.1061/40962(325)7.

Marzouk, I., Oberhollenzer, S., Tschuchnigg, F., 2023a. An automated system for determining soil parameters: Case study. In: Proceedings of the 8th International Symposium on Deformation Characteristics of Geomaterials, Porto.

Marzouk, I., Tschuchnigg, F., Brinkgreve, R.B.J., 2023b. Expansion of an automated system for determining soil parameters using in-situ tests. In: Proceedings of the 10th European Conference on Numerical Methods in Geotechnical Engineering (NUMGE 2023), London. http://dx.doi.org/10.53243/NUMGE2023-70.

Mayne, P.W., 2001. Stress-strain-strength-flow parameters from enhanced in situ tests. In: International Conference on in Situ Measurement of Soil Properties & Case Histories.

Mayne, P.W., 2007. In-situ test calibrations for evaluating soil parameters. In: Characterisation and Engineering Properties of Natural Soils.

Mayne, P.W., 2014. Interpretation of geotechnical parameters from seismic piezocone tests.

Mayne, P.W., 2016. Evaluating effective stress parameters and undrained shear strengths of soft-firm clays from CPTu and DMT. In: Fifth International Conference on Geotechnical and Geophysical Site Characterization. ISC'5.

Mayne, P.W., 2017. Stress history of soils from cone penetration tests. Soils Rocks (3).

Mayne, P.W., Cargil, E., Greig, J., 2023. A CPT Design Parameter Manual. ConeTec Group.

Mayne, P.W., Coop, M., Springman, S., Huang, A.B., Zornberg, J., 2009. State-of-the-art paper (SOA-1): geomaterial behavior and testing.

Mayne, P.W., Rix, G.J., 1995. Correlations between shear wave velocity and cone tip resistance in natural clays. Soils Found. 35 (2), 107–110. http://dx.doi.org/10.3208/sandf1972.35.2_107.

Mayne, P., Robertson, P.K., Lunne, T., 1988. Clay stress history evaluated from seismic piezocone tests. In: Proceedings of the 1st. International Conference on Geotechnical Site Characterisation. Atlanta, Georgia.

Mesri, G., Hayat, T., 1993. The coefficient of earth pressure at rest. Can. Geotech. J. 30 (4), 647–666. http://dx.doi.org/10.1139/t93-056.

Mitchell, J.K., 1976. Fundamentals of Soil Behavior. John Wiley and Sons, New York.

Monaco, P., Amoroso, S., Marchetti, S., Marchetti, D., Totani, G., Cola, S., Simonini, P., 2014. Overconsolidation and stiffness of venice lagoon sands and silts from SDMT and CPTU. J. Geotech. Geoenviron. Eng. 140 (1), 215–227. http://dx.doi.org/10.1061/(ASCE)GT.1943-5606.0000965.

Muir Wood, D., 1990. Soil Behaviour and Critical State Soil Mechanics. Cambridge University Press, Cambridge England and New York, http://dx.doi.org/10.1017/CBO9781139878272.

Ozer, A.T., Bartlett, S.F., Lawton, E.C., 2012. CPTU and DMT for estimating soil unit weight of lake bonneville clay. In: Proceedings of the 4th International Conference on Site Characterization 4, ISC-4, Porto de Galinhas, Brazil. pp. 291–296.

Paniagua, P., D'Ignazio, M., L'Heureux, J.-S., Lunne, T., Karlsrud, K., 2019. CPTU correlations for norwegian clays: An update. AIMS Geosci. 5 (2), 82–103. http://dx.doi.org/10.3934/geosci.2019.2.82.

Phoon, K.K., Kulhawy, F.H., 1999a. Characterization of geotechnical variability. Can. Geotech. J. 36 (4), 612–624. http://dx.doi.org/10.1139/t99-038.

Phoon, K.K., Kulhawy, F.H., 1999b. Evaluation of geotechnical property variability. Can. Geotech. J. 36 (4), 625–639. http://dx.doi.org/10.1139/t99-039.

Powell, J.J.M., Uglow, I.M., 1989. The interpretation of the Marchetti Dilatometer Test in UK clays. Publication of: Telford (Thomas) Limited.

Ramsey, N., Tho, K., 2022. New methods for assessing plasticity index and low-strain shear modulus in fine-grained offshore soils. In: Gottardi, G., Tonni, L. (Eds.), Cone Penetration Testing 2022. CRC Press, pp. 657–663. http://dx.doi.org/10.1201/9781003308829-96.

Robertson, P.K., 2009. Interpretation of cone penetration tests — A unified approach. Can. Geotech. J. 46 (11), 1337–1355. http://dx.doi.org/10.1139/T09-065.

Robertson, P.K., 2010. Soil behaviour type from the CPT: An update. In: 2nd International Symposium on Cone Penetration Testing, Huntington Beach 2. pp. 575–583.

Robertson, P.K., 2015. Guide to cone penetration testing for geotechnical engineering. In: Proceedings of the 3rd International Symposium on Cone Penetration Testing (CPT14, Las Vegas).

Robertson, P.K., 2016. Cone penetration test (CPT)-based soil behaviour type (SBT) classification system — An update. Can. Geotech. J. 53 (12), 1910–1927. http://dx.doi.org/10.1139/cgj-2016-0044.

Robertson, P.K., Cabal, K.L., 2010. Estimating soil unit weight from CPT. In: Proceedings, 2nd International Symposium on Cone Penetration Testing, Huntington Beach, California, USA.

Schanz, T., Vermeer, P., Bonnier, P., 1999. The hardening soil model: Formulation and verification. In: Beyond 2000 in Computational Geotechnics. pp. 281–296.

Schroeder, K., Andersen, K.H., Tjok, K.M., 2006. Laboratory Testing and Detailed Geotechnical Design of the Mad Dog Anchors. OnePetro, http://dx.doi.org/10.4043/17949-MS.

Shu-Xi, W., 2012. The improved dijkstra's shortest path algorithm and its application. Procedia Eng. 29, 1186–1190. http://dx.doi.org/10.1016/j.proeng.2012.01.110.

Sridharan, A., Nagaraj, H.B., 2000. Compressibility behaviour of remoulded, fine-grained soils and correlation with index properties. Canadian Geotechnical Journal 37 (3), 712–722. http://dx.doi.org/10.1139/t99-128.

Taboada, V.M., Espinosa, E., Carrasco, D., Barrera, P., Cruz, D., Gan, K.C., 2013. Predictive equations of shear wave velocity for bay of campeche clay. In: Offshore Technology Conference. http://dx.doi.org/10.4043/24068-MS.

Tanaka, H., Tanaka, M., 1998. Characterization of sandy soils using CPT and DMT. Soils Found. 38 (3), 55–65. http://dx.doi.org/10.3208/sandf.38.3_55.

Van Berkom, I.E., Brinkgreve, R.B.J., Lengkeek, H.J., de Jong, A.K., 2022. An automated system to determine constitutive model parameters from in situ tests. In: Proceedings of the 20th International Conference on Soil Mechanics and Geotechnical Engineering, Sydney 2021.

Vanmarcke, E.H., 1977. Probabilistic modeling of soil profiles. J. Geotech. Eng. Div. 103 (11), 1227–1246. http://dx.doi.org/10.1061/AJGEB6.0000517.

Vanmarcke, E., 1983. Random Fields, Analysis and Synthesis. MIT Press, Cambridge Mass..

Yoon, G.L., Kim, B.T., Jeon, S.S., 2004. Empirical correlations of compression index for marine clay from regression analysis. Canadian Geotechnical Journal 41 (6), 1213–1221. http://dx.doi.org/10.1139/t04-057.

Further reading

Abbasi, N., Javadi, A., Bahramloo, R., 2012. Prediction of compression behaviour of normally consolidated fine-grained soils. World Applied Sciences Journal 18 (1), 06–14.

Abdrabbo, F.M., Mahmoud, M.A., 1990. Correlations Between Index Tests and Compressibility of Egyptian Clays. Soils and Foundations 30 (2), 128–132. http://dx.doi.org/10.3208/sandf1972.30.2_128.

Azzouz, A.S., Krizek, R.J., Corotis, R.B., 1976. Regression Analysis of Soil Compressibility. Soils and Foundations 16 (2), 19–29. http://dx.doi.org/10.3208/sandf1972.16.2_19.

Kalantary, F., 2012. Prediction of compression index using artificial neural network. Scientific Research and Essays 7 (31), http://dx.doi.org/10.5897/SRE12.297.

Kogure, K., Ohira, Y., 1977. Statistical forecasting of compressibility of peaty ground. Canadian Geotechnical Journal 14 (4), 562–570. http://dx.doi.org/10.1139/t77-057.

Lav, M.A., Ansal, A.M., 2001. Regression analysis of soil compressibility. Turkish Journal of Engineering and Environmental Sciences 25 (2), 101–109.

Nakase, A., Kamei, T., Kusakabe, O., 1988. Constitutive Parameters Estimated by Plasticity Index. Journal of Geotechnical Engineering 114 (7), 844–858. http://dx.doi.org/10.1061/(ASCE)0733-9410(1988)114:7(844).

Nishida, Y., 1956. A Brief Note on Compression Index of Soil. Journal of the Soil Mechanics and Foundations Division 82 (3), 1027–1–1027–14. http://dx.doi.org/10.1061/JSFEAQ.0000015.

Park, H.I., Lee, S.R., 2011. Evaluation of the compression index of soils using an artificial neural network. Computers and Geotechnics 38 (4), 472–481. http://dx.doi.org/10.1016/j.compgeo.2011.02.011.

Tiwari, B., Ajmera, B., 2012. New Correlation Equations for Compression Index of Remolded Clays. Journal of Geotechnical and Geoenvironmental Engineering 138 (6), 757–762. http://dx.doi.org/10.1061/(ASCE)GT.1943-5606.0000639.

Vinod, P., Bindu, J., 2010. Compression index of highly plastic clays-an empirical correlation. Indian Geotechnical Journal 40 (3), 174–180.

Wroth, C.P., Wood, D.M., 1978. The correlation of index properties with some basic engineering properties of soils. Canadian Geotechnical Journal 15 (2), 137–145. http://dx.doi.org/10.1139/t78-014.